ROS signaling by NOX4 drives fibroblast-to-myofibroblast differentiation in the diseased prostatic stroma

Natalie Sampson[1], Rafal Koziel[1], Christoph Zenzmaier[1], Lukas Bubendorf[2], Eugen Plas[3], Pidder Jansen-Dürr[1] & Peter Berger[1]*

[1] Institute of Biomedical Aging Research, Austrian Academy of Science, Innsbruck, Austria

[2] Institute of Pathology, University Hospital Basel, Basel, Switzerland

[3] Ludwig Boltzmann Institute for Andrology and Urology, Hospital Lainz, Vienna, Austria

*__Corresponding author:__

Tel +43 512 58391924

Fax +43 512 583919-8

Email peter.berger@oeaw.ac.at

Disclosure summary: the authors have no potential conflicts of interest

Running title: NOX4 drives prostatic stromal remodeling

Keywords:

benign prostatic hyperplasia, insulin-like growth factor binding protein 3, prostate cancer, selenium, transforming growth factor beta-1

Non-standard abbreviations:

BPH, benign prostatic hyperplasia; CM-H_2DCF-DA, 5-(and-6)-chloromethyl-2',7'-dichlorodihydrofluorescein diacetate, acetyl ester; ctFBS, charcoal-treated fetal calf serum; DHE, dihydroethidium; DPI, diphenylene iodonium; ECM, extracellular matrix; GPX3, Glutathione peroxidase 3; IGFBP3, Insulin-like growth factor binding protein 3; MAPK, mitogen-activated protein kinase; NOX, NADPH oxidase; qPCR, quantitative PCR; PCa, prostate cancer; PrSC, primary prostatic stromal cell; Se-Cys, selenocysteine; SEPP1, Selenoprotein P plasma 1; SOD, superoxide dismutase; TXN, Thioredoxin; TXNRD1, Thioredoxin reductase 1.

ABSTRACT

Stromal remodeling, in particular fibroblast-to-myofibroblast differentiation, is a hallmark of benign prostatic hyperplasia (BPH) and solid tumors, including prostate cancer (PCa). Increased local production of TGFbeta1 is considered the inducing stimulus. Given that stromal remodeling actively promotes BPH/PCa development, there is considerable interest in developing stromal-targeted therapies. Microarray and quantitative PCR analysis of primary human prostatic stromal cells (PrSCs) induced to undergo fibroblast-to-myofibroblast differentiation with TGFbeta1 revealed up-regulation of the ROS producer NADPH oxidase 4 (NOX4) and down-regulation of the selenium-containing ROS scavenging enzymes Glutathione peroxidase 3 (GPX3), Thioredoxin reductase 1 (TXNRD1) and the selenium transporter Selenoprotein P plasma 1 (SEPP1). Consistently, NOX4 expression correlated specifically with the myofibroblast phenotype *in vivo* and loss of SEPP1 was observed in tumor-associated stroma of human PCa biopsies. Using lentiviral NOX4 shRNA-mediated knockdown, pharmacological inhibitors, antioxidants and selenium, we demonstrate that TGFbeta1 induction of NOX4-derived ROS is required for TGFβ1-mediated phosphorylation of JNK, which in turn is essential for subsequent downstream cytoskeletal remodeling. Significantly, selenium supplementation inhibited differentiation by increasing ROS scavenging selenoenzyme biosynthesis since GPX3 and TXNRD1 expression and TXNRD1 enzyme activity were restored. Consistently, selenium depleted ROS levels downstream of NOX4 induction. Collectively, this work demonstrates that dysregulated redox homeostasis driven by elevated NOX4-derived ROS signaling underlies fibroblast-to-myofibroblast differentiation in the diseased prostatic stroma. Further, these data indicate the potential clinical value of selenium and/or NOX4 inhibitors in preventing the functional pathogenic changes of stromal cells in BPH and PCa.

INTRODUCTION

Benign prostatic hyperplasia (BPH) and prostate cancer (PCa) are two of the most common diseases affecting aging males (1-3). Although distinct pathologies, BPH and PCa are both associated with changes in the stromal microenvironment that actively promote disease development (4, 5). In particular, the BPH and PCa-adjacent stroma (the latter also termed reactive stroma) are characterized by increased extracellular matrix (ECM) deposition, capillary density and differentiation of fibroblast into myofibroblasts, whose mitogenic secretome promotes proliferation, angiogenesis and tumorigenesis (6-9). Initial treatments for BPH and local-confined PCa target androgen signaling/metabolism resulting in apoptosis of androgen-dependent cells and reduced prostate volume (10, 11). However, neither approach specifically addresses the stromal component of disease. Understanding the mechanisms underlying stromal remodeling in particular fibroblast-to-myofibroblast differentiation may facilitate the development of preventive or more effective treatment strategies.

Elevated production of the cytokine TGFbeta1 (TGFβ1) is observed in BPH and pre-tumorigenic prostatic lesions with tissue and circulating levels positively correlating with disease risk and more rapid PCa progression (12, 13). We and others demonstrated that TGFβ1 induces fibroblast-to-myofibroblast differentiation and stromal remodeling both *in vitro* and *in vivo* (14-16). TGFβ1 is thus considered a key inducer of pathogenic stromal reorganization, however its downstream molecular effectors and hence potential therapeutic targets remain unknown.

Excessive levels of reactive oxygen species (ROS) are associated with the pathology of many human diseases. By contrast, various cellular stimuli (e.g. growth factors, cytokines and hormones) induce the regulated production of low levels of ROS. In such cellular contexts, ROS act as signaling messengers regulating diverse physiological processes via reversible oxidative modification of lipids, DNA and specific cysteine residues of susceptible proteins (e.g. transcription factors, protein tyrosine kinases, and protein tyrosine phosphatases) resulting in altered activity and function (17).

The NADPH oxidase (NOX) family is a major source of intracellular ROS (18). NOX enzymes catalyze the reduction of oxygen using cytosolic NADPH as an electron donor generating superoxide, which may undergo subsequent dismutation to hydrogen peroxide. Of the seven NOX enzymes in

humans, NOX1 and NOX2 play a role in host defense whereas ROS produced by other NOX enzymes act primarily as signaling molecules (19). Dysregulated NOX4 expression is implicated in differentiation associated with cardiac fibrosis and idiopathic lung pulmonary fibrosis (20, 21). However, the molecular mechanism by which NOX4-derived ROS directed differentiation was not identified.

The potentially damaging effects of ROS are limited by antioxidant systems, such as glutathione peroxidases (GPXs) and thioredoxin reductases (TXNRDs). An integral component of GPX and TXNRD enzymes is the essential trace element selenium (Se), which is incorporated as seleno-cysteine (Se-Cys) at their active site (22). The expression and biosynthesis of such selenoproteins is determined by Se status in a strict hierarchical manner (23, 24). Due to its high levels in plasma and an unusually high Se-Cys content, Selenoprotein P plasma 1 (SEPP1) is primarily thought to function as a Se transporter (25).

We demonstrate that TGFβ1-mediated fibroblast-to-myofibroblast differentiation of primary human prostatic stromal cells (PrSCs) is driven via induction of NOX4/ROS signaling. NOX4/ROS induce the phosphorylation of JNK, which subsequently activates the downstream transcriptional program of differentiation. Elevated ROS signaling is supported by the concomitant down-regulation of selenium-containing ROS scavenging enzymes and the selenium transporter SEPP1. Selenium supplementation restored expression of selenium-containing ROS scavengers, increased TXNRD1 activity, depleted NOX4-derived ROS levels and attenuated differentiation. The potential clinical value of selenium and/or NOX4 inhibitors in preventing the transformation of stromal cells in BPH and PCa is indicated.

RESULTS

Dysregulation of redox-regulators during prostatic fibroblast differentiation

To investigate the molecular changes during BPH/PCa-associated fibroblast-to-myofibroblast differentiation the expression profiles of TGFβ1-induced differentiated and non-differentiated PrSCs were analyzed by Affymetrix microarray. 1611 genes were identified with at least 2.5 fold change in their expression levels. Consistent with previous reports a significant proportion of regulated genes encoded ECM components or enzymes involved in ECM remodeling (9, 15) (Supplemental Table 1). One of the most strongly induced genes was *NOX4* (436.6 ± 20.8 fold). Of the other known NOX and associated genes, the regulatory phox subunit $p67^{phox}$ (*NCF2*) was also significantly up-regulated. In addition, several genes encoding proteins with ROS scavenging function were significantly down-regulated, including *Selenoprotein P plasma 1* (*SEPP1), Glutathione peroxidase 3 (GPX3), Thioredoxin (TXN)* and *Thioredoxin reductase 1 (TXNRD1)* (supplemental Table 1). These data were verified by quantitative PCR (qPCR; Fig. 1). The superior sensitivity of qPCR over microarray for the detection of low abundance transcripts revealed that despite their very low basal expression (ct value <35) *NOX1* and *NOX5* were marginally but significantly down-regulated during TGFβ1-induced differentiation (-2.8 ± 0.4 and -2.9 ± 0.4 fold, respectively, p-value = 0.0005). *NOX2* or *NOX3* were not detectably expressed in PrSCs (not shown). These data suggest that TGFβ1-induced differentiation of PrSCs is associated with a NOX4-driven pro-oxidant shift in redox homeostasis.

NOX4 expression correlates with the myofibroblast phenotype *in vivo*

NOX4 expression was verified by qPCR in non-tumor containing small prostate samples derived from radical prostatectomies (n = 13, Fig. 1B) and compared to the expression of a panel of epithelial-, stromal- and myofibroblast-specific markers (Fig. 1C). *NOX4* exhibited no correlation with 8 epithelial markers but weakly correlated with 6 stromal markers (R^2 = 0.21) and more strongly with 5 different myofibroblast markers (R^2 = 0.76). Thus, consistent with our observation from *in vitro* induced fibroblast-to-myofibroblast differentiation of PrSCs, NOX4 mRNA levels specifically correlate with the myofibroblast phenotype *in vivo*.

Specific loss of SEPP1 in tumor-associated stroma of human prostate biopsies

Down-regulation of the Se transporter *SEPP1* during differentiation (-14.2 ± 2.8 fold by qPCR; Fig. 1A) was confirmed at the protein level in cell lysates by Western blotting (-2.4 ± 0.2 fold; Fig. 1D). Moreover, secreted SEPP1 could be detected in the culture media from prostatic fibroblasts but not in the supernatants from TGFβ1-induced differentiated PrSCs (Fig. 1D).

To determine whether loss of SEPP1 is associated with pathogenic stromal remodeling *in vivo*, prostate biopsies from normal/BPH and PCa patients were stained for SEPP1 by immunohistochemistry (Fig. 1E). Specificity of the SEPP1 signal was verified by pre-blocking with a peptide corresponding to residues 244-258 of human SEPP1 against which the antibody was raised (Fig. 1E) (26). In normal prostate (n = 12), strong SEPP1 cytoplasmic staining was observed in basal and luminal epithelial cells and smooth muscle cells (SMCs). Periglandular stromal cells (fibroblasts, perivascular and endothelial cells) were moderately stained (Fig. 1E). However, in biopsies of PCa patients (Gleason 7, n = 8) SEPP1 immunoreactivity was specifically lost in the periglandular tumor-associated (reactive) stroma whereas adjacent bundles of smooth muscle and tumor cells stained positive (Fig. 1E). Thus, consistent with the reduction of SEPP1 in differentiated PrSCs, the remodeled prostatic stroma in PCa exhibits specific loss of stromal SEPP1.

Elevated ROS production precedes fibroblast differentiation

To determine the functional significance of TGFβ1-induced NOX4 expression and suppression of ROS scavengers, ROS production was measured in PrSCs via luminol-based chemiluminescence and using the intracellular probes dihydroethidium (DHE) and 5-(and-6)-chloromethyl-2',7'-dichlorodihydrofluorescein diacetate, acetyl ester (CM-H_2DCFDA) (Fig. 2A-B and data not shown). In comparison to basic fibroblast growth factor (bFGF) treated control cells, TGFβ1-differentiated PrSCs produced significantly elevated ROS levels (2.6 fold ±0.1 by H_2DCFDA and 10.2 fold ±1.7 by luminol), which could be rapidly ablated with the NOX inhibitor diphenylene iodonium (DPI) (Fig. 2A). No significant change in ROS levels was observed upon PrSC stimulation with phorbol 12-myristate 13-acetate or ionomycin, which induce NOX1 and NOX5 activity, respectively (not shown).

This is consistent with their low expression in PrSCs (as before) and indicates that NOX1 and NOX5 do not significantly contribute to the elevated ROS detected during differentiation.

In agreement with tetracycline-inducible NOX4 systems (27), elevated ROS production began 2-6 h after addition of TGFβ1. Peak levels were reached at 12 h and remained steady thereafter (Fig. 2C). Cycloheximide completely abolished TGFβ1-mediated induction of ROS production indicating de novo protein synthesis is required (not shown). Elevated ROS production closely correlated with temporal induction of NOX4 expression, whereas up-regulation of differentiation markers Smooth Muscle Cell Actin (SMA, ACTG2) and Insulin-like growth factor binding protein 3 (IGFBP3) occurred later (12-24 h; Fig. 2C), a finding confirmed at the protein level (Fig. 2D). Thus, TGFβ1-dependent *NOX4* induction and elevated intracellular ROS production precede PrSC differentiation.

Elevated ROS during differentiation do not impose major global DNA damage or protein oxidation

When cellular ROS scavenging activity is deficient, high ROS levels may induce non-specific damage to DNA, proteins and lipids via irreversible oxidation, termed oxidative stress (28). We therefore analyzed the impact of TGFβ1-induced NOX4 activity on γH2A.X levels and the degree of protein carbonylation as markers of genome-wide DNA damage and oxidation in the cellular proteome, respectively (29, 30). Whilst there was a marginal increase in γH2A.X levels (1.3 fold) during TGFβ1-mediated differentiation, the degree of DNA damage was significantly lower ($p = 0.0002$) than in hydrogen peroxide control treated cells (2.2 fold, $p = 0.0006$) (Fig. 3A). Moreover, no significant change in protein carbonylation was detected in TGFβ1-treated cells relative to bFGF control (Fig. 3B). More specifically, only the reduced (active) form of the readily oxidized PTP family member PTEN, which migrates slower under non-reducing SDS-PAGE relative to the oxidized (inactive) phosphatase (31), was present in lysates of PrSCs stimulated for 24 h with bFGF or TGFβ1 (Fig. 3C). Furthermore, in PrSCs incubated for 24-72 h with TGFβ1 there was no significant increase in phosphorylation of p53 at Ser15, which serves as an early indicator of oxidative-stress induced DNA damage (32) (Fig. 3D). Thus, despite sustained elevated ROS levels and reduced expression of ROS

scavenging enzymes, ROS produced in response to TGFβ1 do not impose major global DNA damage or protein oxidation.

Elevated ROS are essential for fibroblast-to-myofibroblast differentiation

ROS produced in response to growth factors and cytokines are emerging as important second signaling messengers. We therefore investigated whether the elevated ROS produced in response to TGFβ1 are required for PrSC differentiation. To this end, the antioxidant enzyme superoxide dismutase (SOD) conjugated to polyethylene glycol (PEG) to enhance cell permeation was employed. SOD, which catalyzes the dismutation of superoxide into H_2O_2 and O_2, significantly reduced TGFβ1-induced ROS levels as determined by luminol-based chemiluminescence (Fig. 4A). Moreover, SOD inhibited induction of the differentiation markers IGFBP3 and SMA and phenotypic switching (Fig. 4B-C). These data provide key evidence that ROS, most likely superoxide, are essential for TGFβ1-induced differentiation in PrSCs.

NOX4 is essential for fibroblast-to-myofibroblast differentiation

To confirm that NOX4 is the ROS-producing source in response to TGFβ1, NOX4-specific lentiviral-delivered shRNA was employed (Fig. 5A). NOX4 shRNA dose-dependently reduced basal *NOX4* expression and significantly attenuated TGFβ1-induced *NOX4* expression (45.9 ±4.7 fold in vector and scrambled control cells) to just 8.3 ± 2.8 fold (MOI 2; Fig. 5B). Expression of the weakly detectable *NOX1* and *NOX5* was not significantly altered (not shown). Due to the limited availability of NOX4-specific immunological agents (33), it was not possible to verify NOX4 knockdown at the protein level.

We next investigated whether NOX4 silencing reduced TGFβ1-induced ROS production. Indeed, NOX4 knockdown reduced TGFβ1-induced ROS levels by 64.9% ± 9.1 (Fig. 5C). Residual ROS levels were most likely due to incomplete silencing of NOX4 since higher levels of NOX4 lentivirus (MOI 5) further reduced TGFβ1-induced ROS production (not shown). However, cell viability was impaired at MOI >6, which is consistent with a threshold basal level of NOX4-derived ROS being essential for cell survival (34, 35). Subsequent experiments thus employed lentivirus at MOI 2. Under

these conditions, NOX4 knockdown significantly attenuated TGFβ1-induction of differentiation markers IGFBP3 and SMA at the mRNA (-3.7 ± 0.2 and -2.5 ± 0.4 fold, respectively; Fig. 5B) and protein level (Fig. 5D) compared to vector and scrambled control cells. Basal IGFBP3 and SMA mRNA and protein levels were not affected by NOX4 knockdown (Fig. 5A and 5D, respectively). The morphological changes of PrSC fibroblast-to-myofibroblast differentiation (15) were also inhibited upon NOX4 silencing (not shown). Collectively, these data establish NOX4 as the predominant ROS-producing source induced by TGFβ1 in PrSCs and an essential mediator of fibroblast-to-myofibroblast differentiation.

NOX4 induces JNK phosphorylation to mediate differentiation

The intracellular response to cytokines including TGFβ1 is transduced by the concerted action of numerous kinases and phosphatases, whose activity is frequently redox-sensitive (17). We therefore examined the effect of NOX4 silencing on the phosphorylation status of different kinases during differentiation. TGFβ1-induced phosphorylation of PKC and PKB/AKT was not perturbed by NOX4 knockdown and p38 MAPK was not detectably phosphorylated in PrSCs before or after differentiation (not shown). However, NOX4 silencing reduced TGFβ1-stimulated but not basal phosphorylation of JNK (Fig. 5D).

Using a JNK-specific inhibitor (SP600125), we examined the requirement of JNK during differentiation. Whilst there was no significant change in TGFβ1-induction of *NOX4* mRNA (Fig. 5E), TGFβ1-induction of IGFBP3 and SMA and morphological differentiation were inhibited by SP600125 (Fig. 5F and data not shown). Collectively, these data indicate that NOX4 is required for JNK phosphorylation, which in turn coordinates the downstream differentiation response to TGFβ.

Selenium attenuates differentiation by restoring ROS scavenging seleno-enzyme activity

The above data suggest that abrogating NOX4-derived ROS signaling may represent a therapeutic strategy to inhibit fibroblast-to-myofibroblast differentiation in BPH and PCa, however there are currently no NOX4-specific inhibitors. We therefore examined whether exogenous Se was sufficient to restore expression/activity of selenium-containing ROS scavenging enzymes and thereby abrogate

NOX4-derived ROS signaling to inhibit differentiation. Subcytotoxic concentrations (5 nM) of selenium as inorganic sodium selenite significantly increased basal expression of *TXN* and the selenoenzymes *GPX3* and *TXNRD1* but not that of non-selenium containing *CAT* (not shown). Moreover, differentiation-associated down-regulation of *GPX3*, *TXN* and *TXNRD1* was completely inhibited, whereas *CAT* expression remained comparable to cells treated with TGFβ1 alone (Fig. 6A). Despite SEPP1 mRNA levels being unchanged by selenite treatment (Fig. 6A), SEPP1 protein levels increased upon addition of selenite (Fig. 6B). In addition, TXNRD1 mRNA and protein levels and enzyme activity were significantly increased upon selenite treatment (TXNRD1 activity 2.0 ± 0.1, p-value 0.004) (Fig. 6B-C).

Consistent with increased selenoenzyme ROS scavenging activity, selenite strongly reduced TGFβ1-induced ROS levels (9.0 ± 3.8 fold, p-value = 0.01) without significantly attenuating TGFβ1 induction of NOX4 mRNA (-2.1 ± 0.3 fold, p-value = 0.07) (Fig. 7A-B). Basal levels of the differentiation markers IGFBP3 and SMA were unaffected by selenite treatment (Fig. 7C and data not shown). However, the attenuation of ROS induction by selenite was sufficient to inhibit TGFβ1-mediated induction of IGFBP3 and SMA at the mRNA and protein level (Fig. 7B-C). In addition, selenite reduced pJNK levels as observed upon NOX4 knockdown. Moreover, selenite inhibited phenotypic switching associated with TGFβ1-induced differentiation (Fig. 7D). Collectively, these data indicate that selenite abrogates the initiated TGFβ1-induced differentiation cascade by restoring the biosynthesis and activity of ROS scavenging selenoenzymes, thereby depleting NOX4-derived ROS and attenuating ROS signaling.

DISCUSSION

Stromal remodeling via fibroblast-to-myofibroblast differentiation promotes the development of BPH and PCa. Elevated production of TGFβ1, a potent inducer of fibroblast differentiation *in vitro* and *in vivo*, is considered the inducing stimulus (15, 16, 36, 37). We demonstrate that ROS signaling by NOX4 induces fibroblast-to-myofibroblast differentiation in PrSCs by increasing phosphorylation of JNK, which coordinates downstream cytoskeletal remodeling and phenotypic differentiation. *NOX4* specifically correlated *in vivo* with the myofibroblast phenotype, the predominant stromal cell type in BPH and PCa. Moreover, loss of the Se transporter SEPP1 was observed in the tumor-associated stroma of PCa biopsies. To our knowledge this is the first report demonstrating dysregulation of redox homeostasis in stromal remodeling in BPH and PCa.

NOX4 is the major source of elevated ROS during TGFβ1-mediated PrSC differentiation as demonstrated by isoform-specific knockdown. The abrogation of differentiation upon depletion of superoxide by SOD demonstrated the critical role of NOX4-derived ROS as mediators of differentiation and moreover, suggested that superoxide is the primary ROS signaling mediator rather than its dismutation product H_2O_2.

In contrast to many peptide growth factors that induce transient ROS production, PrSCs undergoing differentiation produce sustained elevated levels of intracellular ROS as demonstrated using the intracellular redox-sensitive probes DHE and H_2DCFDA. Nonetheless, TGFβ1-differentiated PrSCs do not exhibit major global DNA damage or protein oxidation, indicating that ROS produced in response to TGFβ1 in PrSCs act primarily as intracellular signaling molecules to coordinate differentiation. In addition to the prostate, TGFβ1 as well as other peptide growth factors induces NOX4 expression and ROS production in cells from diverse tissues, including liver, lung, heart and kidney (20, 21, 38). This suggests that NOX4-derived ROS are a common mediator of TGFβ/peptide growth factor signal transduction.

The signaling functions of ROS are primarily mediated by oxidative modification of redox-sensitive proteins, including transcription factors (e.g. NF-κB, AP1, HIF1, p53), protein tyrosine phosphatases and protein tyrosine kinases (17). Typically, ROS inactivate protein tyrosine phosphatases but activate protein tyrosine kinases and thereby promote kinase cascades. Consistently, PrSC differentiation was

associated with NOX4/ROS-dependent phosphorylation of JNK, which was confirmed using pharmacological inhibition to be essential for transducing the TGFβ1 differentiation signal downstream of NOX4. The precise NOX4/ROS target(s) that is responsible for elevated JNK phosphorylation remain to be identified, however, during differentiation we observed NOX4/ROS-dependent down-regulation of *DUSP10*, which encodes a dual-specificity phosphatase that selectively dephosphorylates JNK and p38 (39) (data not shown). These data would be consistent with the sustained NOX4/ROS-dependent phosphorylation of JNK during differentiation and suggest that NOX4 modulates pJNK levels, at least in part, by targeting transcription factor(s) that regulate the expression of *DUSP* phosphatase(s).

Whilst targeting NOX4-derived ROS signaling directly for therapeutic intervention of PCa/BPH remains a possibility, there are currently no specific NOX4 inhibitors. We therefore explored the alternative strategy of increasing ROS scavenging activity. The primary function of SEPP1 is considered the transport of Se to peripheral tissues, which is required for the expression and biosynthesis of selenoproteins (23, 24, 40-42). Thus, down-regulation of SEPP1 during differentiation, a direct transcriptionally suppressed target of TGFβ1/SMAD (43), may result in cellular Se deficiency, decreased selenoenzyme ROS scavenging activity and thereby potentiate NOX4-derived ROS signaling. Indeed, selenite-mediated inhibition of differentiation was associated with (i) reduced TGFβ-induced ROS without a reduction in *NOX4* mRNA levels, (ii) elevated mRNA levels of the selenoenzymes *GPX3* and *TXNRD1* as reported previously (41, 42, 44), (iii) induced TXNRD1 protein levels and (iv) increased TXNRD1 enzyme activity. Selenite had no effect on *SEPP1* mRNA levels, most likely due to upstream inhibition by TGFβ1/SMAD (43), however SEPP1 protein levels were increased presumably via post-translational mechanisms (45). Collectively, these data suggest that selenite attenuates fibroblast-to-myofibroblast differentiation via enhanced biosynthesis of ROS scavenging selenoenzymes, which depletes TGFβ1-induced NOX4-derived ROS thereby preventing dysregulated NOX4/ROS signaling.

These findings are consistent with a large body of data in experimental animals that Se deficiency or supplementation increase or reduce tumor incidence, respectively (46-48). However, several large-scale clinical and epidemiological studies yielded conflicting results relating plasma Se levels to the

risk of PCa and the protective effect of Se supplementation on PCa incidence (49-52). Clearly, further well-designed studies are required to encompass a number of factors that may have contributed to these inconsistencies e.g. the source and dose of the Se supplement employed, baseline Se levels, individual Se requirements and genetic variations within antioxidant and selenoprotein genes (53, 54). However, together with the data herein the significant reduction in PCa incidence observed in the Nutritional Prevention of Cancer study suggest that Se supplementation may benefit subpopulations in whom activity of disease-relevant selenoenzymes are suboptimal, perhaps due to environmental and/or genetic factors (52, 53).

In summary, NOX4-derived ROS are essential TGFβ1 signaling effectors that induce the phosphorylation of JNK. Thereby, downstream transcriptional cascades are activated leading to prostatic fibroblast-to-myofibroblast differentiation. ROS signaling and differentiation are supported by the concomitant down-regulation of ROS scavenging selenoenzymes, which can be attenuated by the addition of Se. To our knowledge, these data are the first to demonstrate dysregulation of redox homeostasis in pathogenic activation of stromal fibroblasts in age-related proliferative diseases of the prostate and point to the potential clinical benefit of Se supplementation and/or local NOX4 inhibition in stromal-targeted therapy. Given that TGFβ signaling and myofibroblast activation are associated with numerous fibrotic disorders (e.g. idiopathic lung pulmonary fibrosis, nephrogenic systemic fibrosis, hypertrophic scarring, proliferative vitreoretinopathies, atherosclerotic lesions) and tumorigenesis, it will be interesting to see whether similar NOX4-dependent processes are at work.

MATERIALS AND METHODS

Reagents

Reagents were from Sigma Aldrich unless otherwise specified. Human recombinant TGFβ1 was from R&D Systems, kinase inhibitors and concentrations employed were: TGFβ type 1 receptor activin receptor-like kinase ALK5 inhibitor SB431542 (1 μM, Tocris Bioscience), JNK inhibitor SP600125 (1 μM, Calbiochem). Antibodies were obtained as follows: p53, phospho-JNK, TXNRD1 and α-tubulin (Santa Cruz), IGFBP3 and phospho-SMAD2/3 (R&D Systems), β-actin and α-SMA (Sigma), phospho-p53, , -H2A.X and PTEN (Cell Signaling), SEPP1 was a kind gift from Holger Steinbrenner (Düsseldorf, Germany), HRP-conjugated secondary antibodies (Promega).

Primary cell culture

Human primary prostatic fibroblasts (PrSCs) were established from prostate organoids as described previously (15). PrSCs were maintained for routine culture in stromal cell growth medium (SCGM, Lonza) at 37°C in a humidified atmosphere of 5% CO_2. For all experiments cells of passage 2-4 were used directly from culture (not previously frozen). For differentiation, PrSCs were incubated for 12 h in RPMI 1640 (Lonza) supplemented with 1% charcoal-treated FBS (ctFBS; Hyclone) and antibiotics. Cells were subsequently stimulated with either 1 ng/ml bFGF as mock control or 1 ng/ml TGFβ1 for the indicated duration. For kinase/antioxidant inhibition, cells were pretreated for 1 h with the appropriate kinase inhibitor/antioxidant or DMSO/PEG equivalent before stimulation with bFGF or TGFβ1 as indicated. All experiments were performed at least three times with primary cells from different donors.

RNA isolation, cDNA synthesis and qPCR

Prostate samples from the ventral part of the prostate were obtained after radical prostatectomy (n = 13), snap frozen and stored in liquid nitrogen before homogenization and total RNA isolation using TriZol reagent (Invitrogen). Total RNA from PrSCs was isolated using TriFast reagent (PeqLab). cDNA synthesis and qPCR were performed as described (15). Primer sequences are given in Supplementary Table 2. For PrSC experiments cDNA concentrations were normalized by the internal

standard hydroxymethylbilane synthase (HMBS), a moderate copy number housekeeping gene not regulated under the experimental conditions employed. Relative changes in gene expression were calculated as described (55). For prostate samples cDNA concentrations were normalized to HMBS and EEF1A1. NOX4 expression was compared to the geometric mean expression (ct) value of epithelial markers (KLK3, KLK2, DPP4, EHF, CDH1, TMPRSS2, CORO2A and KRT5), stromal markers (SMA, IGF1, TGFB1I1, OGN, CNN1, PAGE4) or myofibroblast markers (COMP, PLN, RARRES1, COL4A1, TNC).

Microarrays

PrSCs from three independent donors incubated overnight in 1% ctFBS/RPMI were stimulated either with 1 ng/ml bFGF as mock control or with 1 ng/ml TGFβ1 for 48 h. 2 μg total RNA from each donor were pooled and hybridization to Affymetrix Human Genome U133 Plus 2.0 GeneChips® was performed at the Microarray Facility (Tübingen, Germany). A technical replicate array was performed. Raw expression data were normalized using the GRCMA algorithm at CARMAweb (56, 57). The complete microarray dataset is available at ArrayExpress (E-MEXP-2167).

Lentiviral-mediated knockdown of NOX4

NOX4, scrambled and empty vector shRNA lentiviral particles were generated as described (58). For viral transduction, PrSCs were seeded in appropriate vessels in SCGM. The following day, media was replenished supplemented with 8 μg/ml polybrene and virus-containing supernatant at the MOI indicated. After 96 h, cells were incubated overnight in 1% ctBCS supplemented RPMI containing antibiotics before stimulation with 1 ng/ml TGFβ1 for the duration indicated. In all experiments, empty pLKO.1 vector and/or scramble shRNA vector (Addgene plasmid 1864) were used as controls.

Determination of ROS production

For luminol-based chemiluminescent ROS detection, 20,000 PrSCs in triplicate in 24well plates were incubated overnight in 1% ctBCS in RPMI before stimulation as indicated. Cell monolayers were rinsed with pre-warmed Hanks' Buffered Salt Solution without Ca^{2+} and Mg^{2+} (HBSS, Lonza) and

incubated with 4 U/ml horseradish peroxidase and 10 μg/ml luminol in HBSS. Luminescence was measured on a Chameleon luminescence counter (HVD Bioscience) at 37°C. Values were normalized against cell number using the Cell Titer Glo Luminescence assay reagent (Promega).

ROS production was also measured via CM-H_2DCFDA in 2 x 10^5 PrSCs seeded in triplicate in 6 cm dishes and differentiated as above. Cells were trypsinized, rinsed in pre-warmed HBSS before loading with 10 μM CM-H_2DCFDA (Invitrogen) in HBSS for 30 min at 37°C. After washing, cells were resuspended in 500 μl HBSS and analyzed by flow cytometry on a FACSCanto™ II (BD Biosciences).

Western blotting and immunohistochemistry

Isolation of total cell lysates and Western blotting were performed as described (15) and normalized for total protein content via Bradford assay (Bio-Rad). Detection of protein carbonylation was performed as described (59). For analysis of PTEN oxidation lysates were prepared in the presence of 10 mM N-ethylmaleimide (NEM) to prevent cysteine oxidation during lysis. Prostate tissue sections from paraffin blocks of formalin-fixed whole biopsy specimens (obtained from the archives of the Institute of Pathology at the University Hospital Basel, Switzerland) were processed for immunohistochemistry as described (60). Where indicated SEPP1 antibody (1:500) was pre-blocked overnight at 4°C in 1% BSA/PBS containing 50μg/ml blocking peptide (244-258aa, Alta Bioscience, UK).

Analysis of oxidative damage to DNA

5 x 10^5 PrSCs seeded in triplicate in 10 cm dishes were incubated overnight in 1% ctBCS in RPMI before stimulation with bFGF or TGFβ1 for 48 h. Histone H2A.X phosphorylated at Ser139 (γH2A.X) was detected via flow-cytometry on a FACSCanto™ II (BD Biosciences) following immunostaining according to the manufacturer's instructions (Cell Signaling). PrSCs treated with non-apoptosis inducing concentrations of H_2O_2 (250 μM for 60 min) served as positive control.

TXNRD1 enzyme activity

4.5 x 10^5 PrSCs seeded in duplicate in 6 cm dishes were differentiated for 48 hrs. Cell monolayers were rinsed in ice-cold PBS before resuspending in 150µl lysis buffer (0.5% Triton X-100, 0.5% deoxycholate, 150 mM NaCl, 10 mM Tris-HCl pH 7.5, 5 mM EDTA and protease inhibitors). Samples were incubated on ice for 30 min before centrifugation at 13,000 rpm for 15 min at 4°C. Cleared supernatants were normalized for total protein content via Bradford assay before determination of TRXND1 activity by a TXNRD1 activity assay kit (Abcam) according to the manufacturer's instructions.

Statistical analysis

Numerical data are presented as mean ±SEM from at least three independent experiments using independent donors. Statistical evaluation was performed using a Student's *t*-test (ns, not significant; *, $p < 0.05$; **, $p < 0.01$).

ACKNOWLEDGEMENTS

The authors gratefully acknowledge Professor Stephan Dirnhofer (University Hospital Basel, Switzerland) for assistance with immunohistochemistry and Dr. Barbara Lener for technical assistance with the generation of NOX4 shRNA lentivirus. This work was supported by the Austrian Science Fund (FWF; NRN S9307-B05 and S9305-B05), NS is the recipient of a Lise Meitner Scholarship (FWF; M903-B05). The authors have no competing financial interests.

REFERENCES

1. Sampson N, Untergasser G, Plas E, Berger P 2007 The ageing male reproductive tract. J Pathol 211:206-218

2. Isaacs JT 1994 Etiology of benign prostatic hyperplasia. Eur Urol 25 Suppl 1:6-9

3. Jemal A, Siegel R, Ward E, Murray T, Xu J, Smigal C, Thun MJ 2006 Cancer statistics, 2006. CA Cancer J Clin 56:106-130

4. Olumi AF, Grossfeld GD, Hayward SW, Carroll PR, Tlsty TD, Cunha GR 1999 Carcinoma-associated fibroblasts direct tumor progression of initiated human prostatic epithelium. Cancer Res 59:5002-5011

5. Barclay WW, Woodruff RD, Hall MC, Cramer SD 2005 A system for studying epithelial-stromal interactions reveals distinct inductive abilities of stromal cells from benign prostatic hyperplasia and prostate cancer. Endocrinology 146:13-18

6. Ao M, Franco OE, Park D, Raman D, Williams K, Hayward SW 2007 Cross-talk between paracrine-acting cytokine and chemokine pathways promotes malignancy in benign human prostatic epithelium. Cancer Res 67:4244-4253

7. Yang F, Tuxhorn JA, Ressler SJ, McAlhany SJ, Dang TD, Rowley DR 2005 Stromal expression of connective tissue growth factor promotes angiogenesis and prostate cancer tumorigenesis. Cancer Res 65:8887-8895

8. Tuxhorn JA, McAlhany SJ, Yang F, Dang TD, Rowley DR 2002 Inhibition of transforming growth factor-beta activity decreases angiogenesis in a human prostate cancer-reactive stroma xenograft model. Cancer Res 62:6021-6025

9. Verona EV, Elkahloun AG, Yang J, Bandyopadhyay A, Yeh IT, Sun LZ 2007 Transforming growth factor-beta signaling in prostate stromal cells supports prostate carcinoma growth by up-regulating stromal genes related to tissue remodeling. Cancer Res 67:5737-5746

10. Tiwari A 2007 Advances in the development of hormonal modulators for the treatment of benign prostatic hyperplasia. Expert Opin Investig Drugs 16:1425-1439

11. Taplin ME 2008 Androgen receptor: role and novel therapeutic prospects in prostate cancer. Expert Rev Anticancer Ther 8:1495-1508

12. Li Z, Habuchi T, Tsuchiya N, Mitsumori K, Wang L, Ohyama C, Sato K, Kamoto T, Ogawa O, Kato T 2004 Increased risk of prostate cancer and benign prostatic hyperplasia associated with transforming growth factor-beta 1 gene polymorphism at codon10. Carcinogenesis 25:237-240

13. Wikstrom P, Stattin P, Franck-Lissbrant I, Damber JE, Bergh A 1998 Transforming growth factor beta1 is associated with angiogenesis, metastasis, and poor clinical outcome in prostate cancer. Prostate 37:19-29

14. Tuxhorn JA, Ayala GE, Smith MJ, Smith VC, Dang TD, Rowley DR 2002 Reactive stroma in human prostate cancer: induction of myofibroblast phenotype and extracellular matrix remodeling. Clin Cancer Res 8:2912-2923

15. Untergasser G, Gander R, Lilg C, Lepperdinger G, Plas E, Berger P 2005 Profiling molecular targets of TGF-beta1 in prostate fibroblast-to-myofibroblast transdifferentiation. Mech Ageing Dev 126:59-69

16. Roberts AB, Sporn MB, Assoian RK, Smith JM, Roche NS, Wakefield LM, Heine UI, Liotta LA, Falanga V, Kehrl JH, et al. 1986 Transforming growth factor type beta: rapid induction of fibrosis

and angiogenesis in vivo and stimulation of collagen formation in vitro. Proc Natl Acad Sci U S A 83:4167-4171

17. Trachootham D, Lu W, Ogasawara MA, Nilsa RD, Huang P 2008 Redox regulation of cell survival. Antiox Redox Signal10:1343-1374

18. Bedard K, Krause KH 2007 The NOX family of ROS-generating NADPH oxidases: physiology and pathophysiology. Physiol Rev 87:245-313

19. Torres M 2003 Mitogen-activated protein kinase pathways in redox signaling. Front Biosci 8:d369-391

20. Cucoranu I, Clempus R, Dikalova A, Phelan PJ, Ariyan S, Dikalov S, Sorescu D 2005 NAD(P)H oxidase 4 mediates transforming growth factor-beta1-induced differentiation of cardiac fibroblasts into myofibroblasts. Circ Res 97:900-907

21. Hecker L, Vittal R, Jones T, Jagirdar R, Luckhardt TR, Horowitz JC, Pennathur S, Martinez FJ, Thannickal VJ 2009 NADPH oxidase-4 mediates myofibroblast activation and fibrogenic responses to lung injury. Nat Med 15:1077-1081

22. Bellinger FP, Raman AV, Reeves MA, Berry MJ 2009 Regulation and function of selenoproteins in human disease. Biochem J 422:11-22

23. Low SC, Grundner-Culemann E, Harney JW, Berry MJ 2000 SECIS-SBP2 interactions dictate selenocysteine incorporation efficiency and selenoprotein hierarchy. Embo J 19:6882-6890

24. Crane MS, Howie AF, Arthur JR, Nicol F, Crosley LK, Beckett GJ 2009 Modulation of thioredoxin reductase-2 expression in EAhy926 cells: implications for endothelial selenoprotein hierarchy. Biochim Biophys Acta 1790:1191-1197

25. Saito Y, Sato N, Hirashima M, Takebe G, Nagasawa S, Takahashi K 2004 Domain structure of bi-functional selenoprotein P. Biochem J 381:841-846

26. Mostert V, Lombeck I, Abel J 1998 A novel method for the purification of selenoprotein P from human plasma. Arch Biochem Biophys 357:326-330

27. Serrander L, Cartier L, Bedard K, Banfi B, Lardy B, Plastre O, Sienkiewicz A, Forro L, Schlegel W, Krause KH 2007 NOX4 activity is determined by mRNA levels and reveals a unique pattern of ROS generation. Biochem J 406:105-114

28. Valko M, Leibfritz D, Moncol J, Cronin MT, Mazur M, Telser J 2007 Free radicals and antioxidants in normal physiological functions and human disease. Int J Biochem Cell Biol 39:44-84

29. Rogakou EP, Pilch DR, Orr AH, Ivanova VS, Bonner WM 1998 DNA double-stranded breaks induce histone H2AX phosphorylation on serine 139. J Biol Chem 273:5858-5868

30. Amici A, Levine RL, Tsai L, Stadtman ER 1989 Conversion of amino acid residues in proteins and amino acid homopolymers to carbonyl derivatives by metal-catalyzed oxidation reactions. J Biol Chem 264:3341-3346

31. Lee SR, Yang KS, Kwon J, Lee C, Jeong W, Rhee SG 2002 Reversible inactivation of the tumor suppressor PTEN by H2O2. J Biol Chem 277:20336-20342

32. Nair VD, Yuen T, Olanow CW, Sealfon SC 2004 Early single cell bifurcation of pro- and antiapoptotic states during oxidative stress. J Biol Chem 279:27494-27501

33. Nauseef WM 2008 Biological Roles for the NOX Family NADPH Oxidases. J Biol Chem 283:16961-16965

34. Peshavariya H, Dusting GJ, Jiang F, Halmos LR, Sobey CG, Drummond GR, Selemidis S 2009 NADPH oxidase isoform selective regulation of endothelial cell proliferation and survival. Naunyn-Schmiedebergs Arch Pharmacol 380:193-204

35. Shono T, Yokoyama N, Uesaka T, Kuroda J, Takeya R, Yamasaki T, Amano T, Mizoguchi M, Suzuki SO, Niiro H, Miyamoto K, Akashi K, Iwaki T, Sumimoto H, Sasaki T 2008 Enhanced expression of NADPH oxidase Nox4 in human gliomas and its roles in cell proliferation and survival. Int J Cancer 123:787-792

36. Kyprianou N, Tu H, Jacobs SC 1996 Apoptotic versus proliferative activities in human benign prostatic hyperplasia. Hum Pathol 27:668-675

37. Cardillo MR, Petrangeli E, Perracchio L, Salvatori L, Ravenna L, Di Silverio F 2000 Transforming growth factor-beta expression in prostate neoplasia. Anal Quant Cytol Histol 22:1-10

38. Sturrock A, Huecksteadt TP, Norman K, Sanders K, Murphy TM, Chitano P, Wilson K, Hoidal JR, Kennedy TP 2007 Nox4 mediates TGF-beta1-induced retinoblastoma protein phosphorylation, proliferation, and hypertrophy in human airway smooth muscle cells. Am J Physiol Lung Cell Mol Physiol 292:L1543-1555

39. Theodosiou A, Smith A, Gillieron C, Arkinstall S, Ashworth A 1999 MKP5, a new member of the MAP kinase phosphatase family, which selectively dephosphorylates stress-activated kinases. Oncogene 18:6981-6988

40. Saito Y, Takahashi K 2002 Characterization of selenoprotein P as a selenium supply protein. Eur J Biochem / FEBS 269:5746-5751

41. Barnes KM, Evenson JK, Raines AM, Sunde RA 2009 Transcript analysis of the selenoproteome indicates that dietary selenium requirements of rats based on selenium-regulated

selenoprotein mRNA levels are uniformly less than those based on glutathione peroxidase activity. J Nutr 139:199-206

42. Clarke C, Baghdadi H, Howie AF, Mason JI, Walker SW, Beckett GJ 2010 Selenium supplementation attenuates procollagen-1 and interleukin-8 production in fat-loaded human C3A hepatoblastoma cells treated with TGFbeta1. Biochim Biophys Acta 1800:611-618

43. Mostert V, Dreher I, Kohrle J, Wolff S, Abel J 2001 Modulation of selenoprotein P expression by TGF-beta(1) is mediated by Smad proteins. BioFactors (Oxford, England) 14:135-142

44. Gallegos A, Berggren M, Gasdaska JR, Powis G 1997 Mechanisms of the regulation of thioredoxin reductase activity in cancer cells by the chemopreventive agent selenium. Cancer Res 57:4965-4970

45. Yang JG, Hill KE, Burk RF 1989 Dietary selenium intake controls rat plasma selenoprotein P concentration. J Nutr 119:1010-1012

46. Pence BC, Delver E, Dunn DM 1994 Effects of dietary selenium on UVB-induced skin carcinogenesis and epidermal antioxidant status. J Investig Dermatol 102:759-761

47. Diwadkar-Navsariwala V, Prins GS, Swanson SM, Birch LA, Ray VH, Hedayat S, Lantvit DL, Diamond AM 2006 Selenoprotein deficiency accelerates prostate carcinogenesis in a transgenic model. Proc Natl Acad Sci U S A 103:8179-8184

48. Selenius M, Rundlof AK, Olm E, Fernandes AP, Bjornstedt M 2010 Selenium and the selenoprotein thioredoxin reductase in the prevention, treatment and diagnostics of cancer. Antiox Redox Signal 12:867-880

49. Li H, Stampfer MJ, Giovannucci EL, Morris JS, Willett WC, Gaziano JM, Ma J 2004 A prospective study of plasma selenium levels and prostate cancer risk. J Natl Cancer Inst 96:696-703

50. Allen NE, Appleby PN, Roddam AW, Tjonneland A, Johnsen NF, Overvad K, Boeing H, Weikert S, Kaaks R, Linseisen J, Trichopoulou A, Misirli G, Trichopoulos D, Sacerdote C, Grioni S, Palli D, Tumino R, Bueno-de-Mesquita HB, Kiemeney LA, Barricarte A, Larranaga N, Sanchez MJ, Agudo A, Tormo MJ, Rodriguez L, Stattin P, Hallmans G, Bingham S, Khaw KT, Slimani N, Rinaldi S, Boffetta P, Riboli E, Key TJ 2008 Plasma selenium concentration and prostate cancer risk: results from the European Prospective Investigation into Cancer and Nutrition (EPIC). Am J Clin Nutr 88:1567-1575

51. Lippman SM, Klein EA, Goodman PJ, Lucia MS, Thompson IM, Ford LG, Parnes HL, Minasian LM, Gaziano JM, Hartline JA, Parsons JK, Bearden JD, 3rd, Crawford ED, Goodman GE, Claudio J, Winquist E, Cook ED, Karp DD, Walther P, Lieber MM, Kristal AR, Darke AK, Arnold KB, Ganz PA, Santella RM, Albanes D, Taylor PR, Probstfield JL, Jagpal TJ, Crowley JJ, Meyskens FL, Jr., Baker LH, Coltman CA, Jr. 2009 Effect of selenium and vitamin E on risk of prostate cancer and other cancers: the Selenium and Vitamin E Cancer Prevention Trial (SELECT). Jama 301:39-51

52. Duffield-Lillico AJ, Dalkin BL, Reid ME, Turnbull BW, Slate EH, Jacobs ET, Marshall JR, Clark LC 2003 Selenium supplementation, baseline plasma selenium status and incidence of prostate cancer: an analysis of the complete treatment period of the Nutritional Prevention of Cancer Trial. BJU Int 91:608-612

53. Rayman MP 2009 Selenoproteins and human health: insights from epidemiological data. Biochim Biophys Acta 1790:1533-1540

54. Zhuo P, Diamond AM 2009 Molecular mechanisms by which selenoproteins affect cancer risk and progression. Biochim Biophys Acta 1790:1546-1554

55. Pfaffl MW 2001 A new mathematical model for relative quantification in real-time RT-PCR. Nucleic Acids Res 29:e45

56. Rainer J, Sanchez-Cabo F, Stocker G, Sturn A, Trajanoski Z 2006 CARMAweb: comprehensive R- and bioconductor-based web service for microarray data analysis. Nucleic Acids Res 34:W498-503

57. Wu Z, Irizarry R, Gentlemen R, Martinez-Murillo F, Spencer F 2004 A model-based background adjustment for oligonucleotide expression arrays. J Am Stat Assoc 99:909917

58. Lener B, Koziel R, Pircher H, Hutter E, Greussing R, Herndler-Brandstetter D, Hermann M, Unterluggauer H, Jansen-Durr P 2009 The Nadph Oxidase Nox4 Restricts the Replicative Lifespan of Human Endothelial Cells. Biochem J

59. Unterluggauer H, Micutkova L, Lindner H, Sarg B, Hernebring M, Nystrom T, Jansen-Durr P 2009 Identification of Hsc70 as target for AGE modification in senescent human fibroblasts. Biogerontology 10:299-309

60. Zenzmaier C, Untergasser G, Hermann M, Dirnhofer S, Sampson N, Berger P 2008 Dysregulation of Dkk-3 expression in benign and malignant prostatic tissue. Prostate 68:540-547

FIGURE LEGENDS

Fig. 1. NOX4 and SEPP1 are associated with stromal remodeling *in vivo*.

(A) qPCR of ROS scavenging (white bars) and ROS producing (black bars) enzymes in PrSCs differentiated with 1 ng/ml TGFβ1 (48h) relative to control cells incubated with 1 ng/ml bFGF (48h) to maintain the fibroblast phenotype. Values represent mean fold change (±SEM) of four independent experiments using different donors. (B-C) *NOX4* expression was evaluated in non-tumor containing human prostate samples. (B) RTPCR of *NOX4* (negative control using water as substrate; positive control using plasmid DNA containing full-length NOX4 cDNA). RTPCR of *HMBS* is shown as loading control. (C) qPCR of *NOX4* in prostate specimens (n =13) relative to the expression of epithelial, stroma or myofibroblast markers as described in Methods. (D) Western blotting of SEPP1 in lysates and supernatants (SN) of PrSCs treated with 1 ng/ml bFGF or TGFβ1 for 48h. β-actin is shown as loading control. A representative blot of three independent experiments is shown. (E) SEPP1 immunohistochemistry (left) in normal/BPH and PCa biopsies (Gleason 7), enlarged images are shown (right), pre-incubation of anti-SEPP1 antibody with blocking peptide (center). Periglandular stromal cells (short black arrows), periglandular tumor stroma (open arrows), SMC bundles (long black arrow), weak immunostaining of SMCs due to incomplete blocking (grey arrow). Sections were counterstained with Mayer's hematoxylin. Tissue specimens were processed in parallel. Images are representative of four independent experiments with specimens from at least eight different donors.

Fig. 2. Sustained ROS production precedes fibroblast-to-myofibroblast differentiation.

(A) ROS production was measured real-time in PrSCs 24 h post stimulation with TGFβ1 or bFGF as control via luminol-based chemiluminescence. Values represent mean of triplicate wells (±SEM). A representative example of at least three experiments using independent donors is shown. (B) ROS production was measured in PrSCs 48 h post stimulation with TGFβ1or bFGF via H_2DCFDA staining and analyzed by FACS. Values represent mean fluorescence of triplicate samples using three different donors in independent experiments. Significance is indicated (** $p < 0.01$). (C) Time course assay of ROS production (left y-axis) and qPCR (right y-axis) of PrSCs stimulated for the indicated duration with TGFβ1. Mean values obtained from at least three experiments using independent donors are

shown (±SEM). (D) Western blotting of lysates from PrSCs stimulated with TGFβ1 for the indicated duration with the antibody shown. Blots are representative of three independent experiments using different donors.

Fig. 3. Elevated ROS production during differentiation do not induce major global DNA damage or protein oxidation.

(A) H2A.X phosphorylated at Ser139 was quantified via flow-cytometry in PrSCs stimulated for 48 h with either bFGF or TGFβ1. *Top panel*, histograms from a single experiment of γH2A.X staining intensity in PrSCs treated as indicated (negative control, omission of primary antibody in bFGF treated samples). Note the increased (right-ward) shift in staining intensity in H_2O_2 relative to bFGF and TGFβ1-treated samples. *Lower panel*, mean values (±SEM) of triplicate samples using different donors in three independent experiments. (B, *top panel*) PrSCs were treated for the indicated duration with either bFGF or TGFβ1 before detection of total protein carbonyl levels via immunoblotting for anti-DNP immunoreactive proteins in cell extracts derivatized with DNPH (negative control, non-derivatized cell lysate from H_2O_2 treated PrSCs). *Lower panel*, densitometric quantification of total protein carbonyl levels in PrSCs treated as before. Mean values (±SEM) of three independent experiments using different donors are shown. Significance is indicated (**, $p< 0.01$; ns, not significant). (C, D) Western blotting of lysates from PrSCs stimulated with bFGF or TGFβ1 for the indicated duration (C, 24 h; D, hours) with the antibody shown. Blots are representative of three independent experiments using different donors. (A-D) As positive control, PrSCs were incubated with bFGF for 24 (B-D) or 48 h (A) before subsequent treatment with 250 μM H_2O_2 for 60 min.

Fig. 4. ROS are essential for fibroblast-to-myofibroblast differentiation

PrSCs were incubated with polyethylene glycol (PEG)-conjugated superoxide dismutase (PEG-SOD, 60 U/ml) and bFGF or TGFβ1 as indicated for 24 h prior to (A) luminol-based chemiluminescent detection of ROS production, (B) Western blotting using the indicated antibodies or (C) phase contrast microscopy (magnification x 40). (A) Values represent the mean (±SEM) of triplicate wells in three independent experiments using different donors. Significance is indicated (*, $p< 0.05$; **, $p< 0.01$; ns,

not significant). (C) Note the thin, elongated and light refractive phenotype of bFGF-treated PrSCs (fibroblasts) in comparison to the flattened and less light refractive morphology of TGFβ1-differentiated PrSCs (myofibroblasts). (B, C) Images are representative of at least four independent experiments using different donors.

Fig. 5. NOX4-derived ROS mediate differentiation via increased JNK phosphorylation.

(A) qPCR of PrSCs infected with the indicated shRNA-expressing lentivirus at MOI 2 (vector and scrambled) or the indicated MOI (NOX4) for 96 h. (B) qPCR of PrSCs infected as above (MOI 2) and subsequently stimulated for 24 h with TGFβ1. (A, B) Mean values (±SEM) of at least three experiments using independent donors are shown relative to non-transduced mock treated PrSCs. (C) luminol-based chemiluminescent detection of ROS production by PrSCs treated as in (B). Values represent mean fold change in ROS production (±SEM) from triplicate wells in at least three experiments using independent donors relative to vector control cells. (D) Western blotting of total cell lysates from PrSCs treated as in (B) in the presence or absence of TGFβ1 for 24 h. A representative example of four independent experiments using different donors is shown. Values denote densitometric quantification of bands from NOX4 shRNA treated lysates relative to combined scores from vector and scrambled shRNA treated lysates (mean ±SEM). (E-F) PrSCs were treated with TGFβ1 and the indicated inhibitor (JNK, 1 μM SP600125; ALK5/TGFβR1, 1 μM SB431542) for 24 h before (E) qPCR of the indicated genes or (B) Western blotting of total cell lysates using the antibodies indicated. (E) Mean values from at least three independent experiments using different donors are shown expressed as percentage (±SEM) relative to mock control treated with TGFβ1 and DMSO equivalent. (F) A representative example of three independent experiments using different donors is shown. Significance is indicated (* $p < 0.05$, ** $p < 0.01$).

Fig. 6. Selenite restores expression and activity of ROS scavenging selenoenzymes.

(A) qPCR of the indicated genes in PrSCs pre-treated for 12 h with 5 nM sodium selenite or mock control in 1% ctBCS/RPMI before stimulation with TGFβ1 for a further 24 h. Values represent mean fold change in gene expression (±SEM) relative to bFGF control (without selenite). (B) Western

blotting of total cell lysates from cells pre-incubated with selenite as in (A) and subsequently stimulated either with bFGF or TGFβ1 as indicated in the presence or absence of selenite for a further 24 h. Blots are representative of three independent experiments using different donors. (C) Mean fold change in TXNRD1 enzyme activity (±SEM) in cell extracts from PrSCs treated with 5 nM selenite relative to mock treated controls. (A-C) Data are derived from at least three independent experiments using different donors. Significance is indicated (** $p < 0.01$, * $p < 0.05$).

Fig. 7. Selenite inhibits TGFβ1-mediated fibroblast-to-myofibroblast differentiation.

PrSCs were pre-treated for 12 h with 5 nM sodium selenite or mock control before stimulation with 1 ng/ml bFGF or TGFβ1 in the presence or absence of selenite for a further 24 h. Cells were subsequently processed for (A) ROS determination via luminol-based chemilumiscence, (B) qPCR of the indicated genes, (C) Western blotting of total cell lysates using the antibodies indicated or (D) phase contrast microscopy (magnification x40). Note the thin, elongated and light refractive phenotype of bFGF-treated PrSCs (fibroblasts) in comparison to the flattened and less light refractive morphology of TGFβ1-differentiated PrSCs (myofibroblasts). (C, D) Images are representative of at least four independent experiments using different donors. (A, B) Values represent mean fold change (±SEM) relative to bFGF control (without selenite) from four independent experiments using different donors. Significance is indicated (** $p < 0.01$, * $p < 0.05$, ns not significant).

Fig.1

A

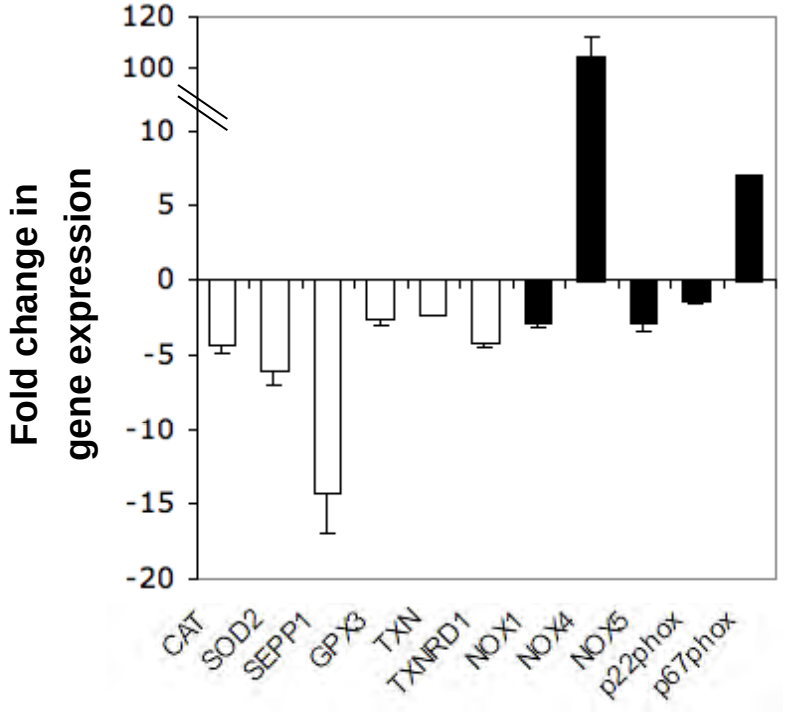
Fold change in gene expression
120
100
10
5
0
-5
-10
-15
-20
CAT
SOD2
SEPP1
GPX3
TXN
TXNRD1
NOX1
NOX4
NOX5
p22phox
p67phox

Fig.1


B
whole prostate
1
2
3
4
5
h2o
NOX4 plasmid
NOX4
HMBS

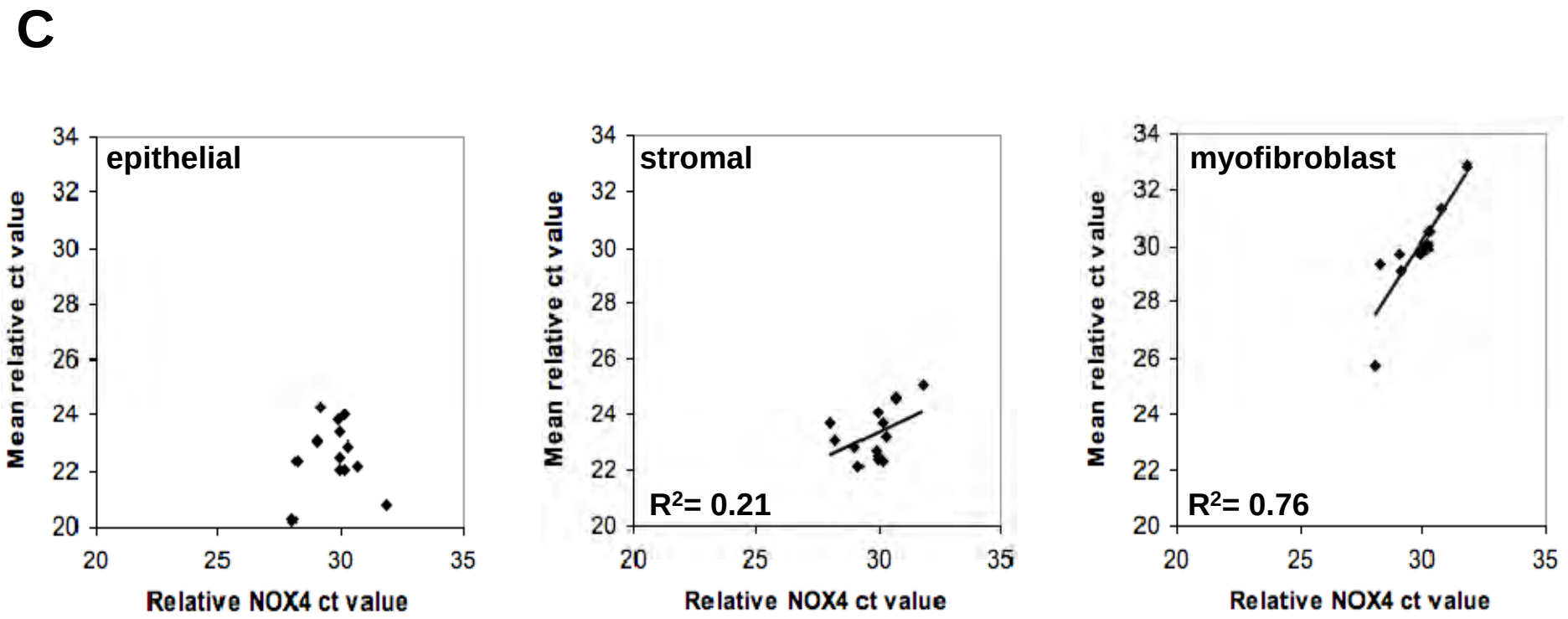
C
epithelial
stromal
myofibroblast
Mean relative ct value
Relative NOX4 ct value
R2= 0.21
R2= 0.76
20
22
24
26
28
30
32
34
20
25
30
35

Fig.1

D

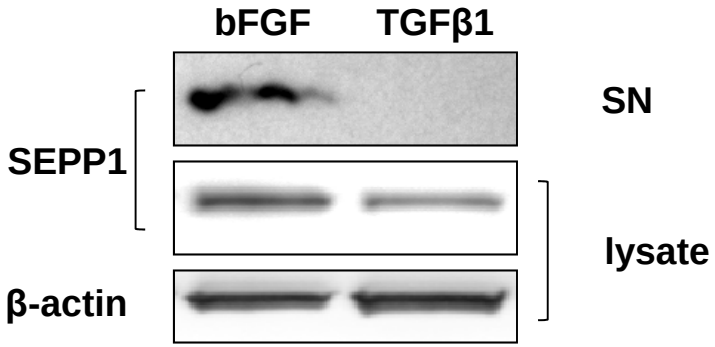
bFGF
TGFβ1
SEPP1
SN
lysate
β-actin

E

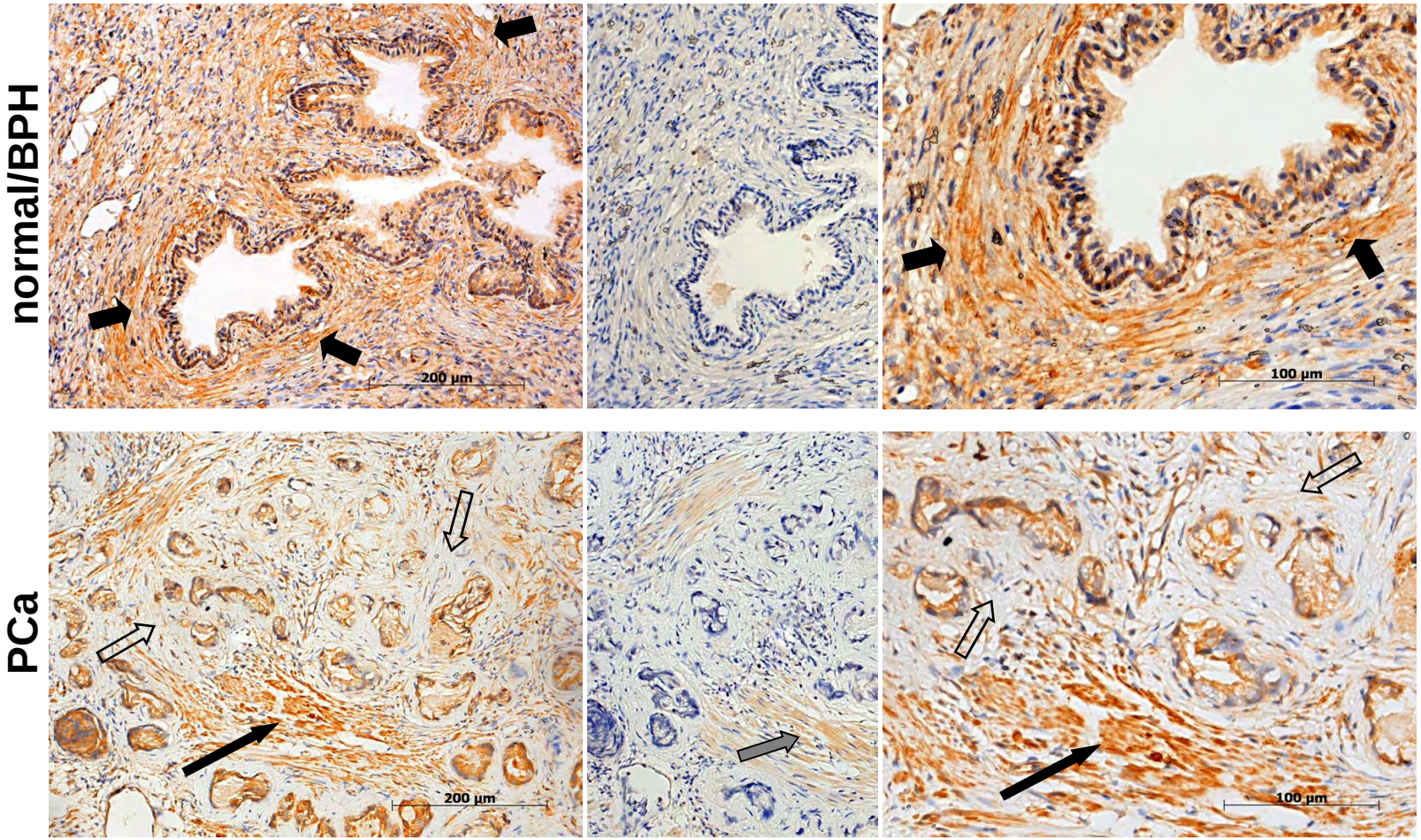
normal/BPH
PCa
200 μm
100 μm
200 μm
100 μm

Fig.2

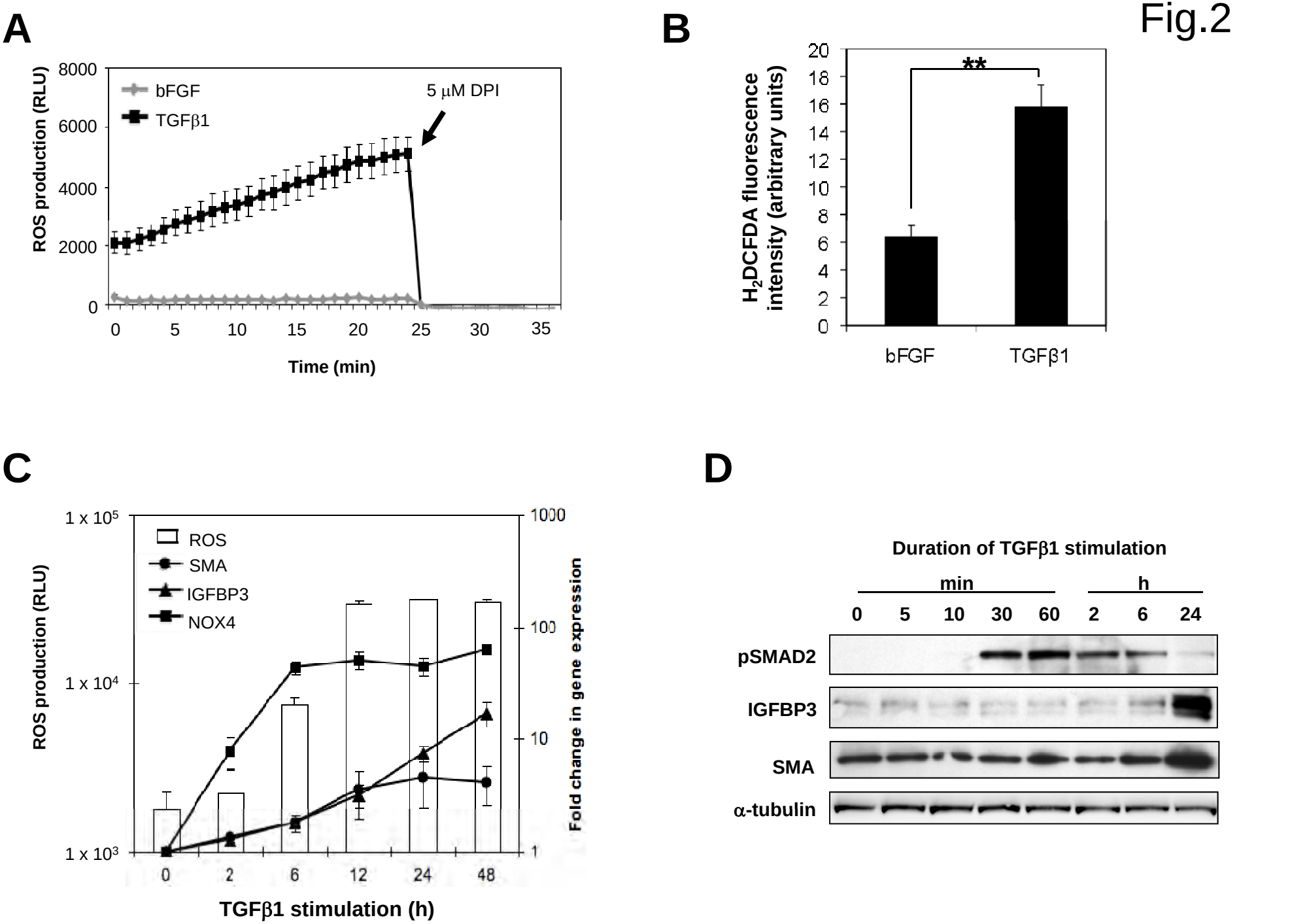
A
ROS production (RLU)
8000
6000
4000
2000
0
bFGF
TGFβ1
5 μM DPI
0
5
10
15
20
25
30
35
Time (min)
B
H2DCFDA fluorescence intensity (arbitrary units)
20
18
16
14
12
10
8
6
4
2
0
**
bFGF
TGFβ1
C
ROS production (RLU)
1 x 10^5
1 x 10^4
1 x 10^3
ROS
SMA
IGFBP3
NOX4
1000
100
10
1
Fold change in gene expression
0
2
6
12
24
48
TGFβ1 stimulation (h)
D
Duration of TGFβ1 stimulation
min
h
0
5
10
30
60
2
6
24
pSMAD2
IGFBP3
SMA
α-tubulin

Fig. 3

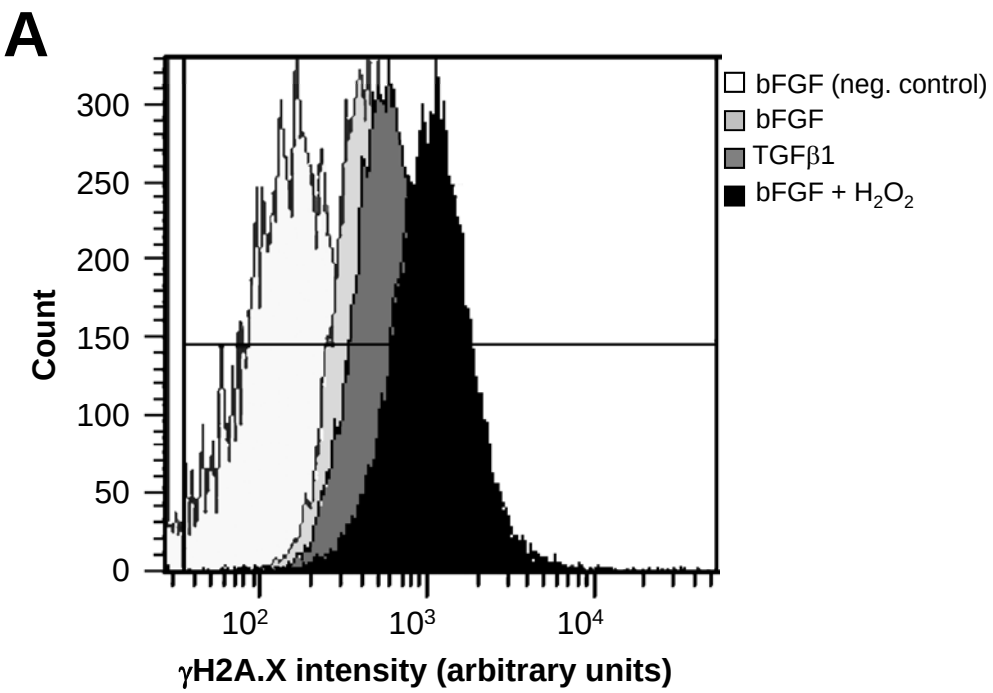
A
bFGF (neg. control)
bFGF
TGFβ1
bFGF + H2O2
Count
300
250
200
150
100
50
0
10^2
10^3
10^4
γH2A.X intensity (arbitrary units)

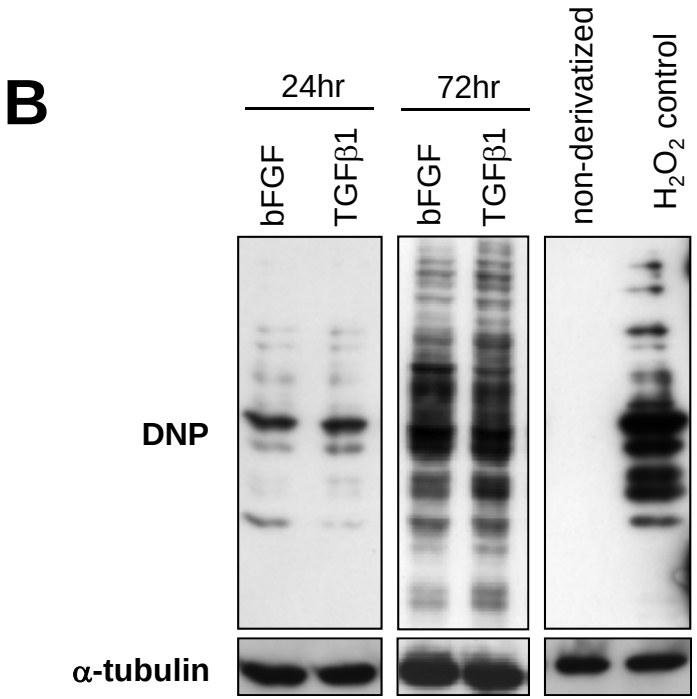
B
24hr
72hr
bFGF
TGFβ1
bFGF
TGFβ1
non-derivatized
H2O2 control
DNP
α-tubulin

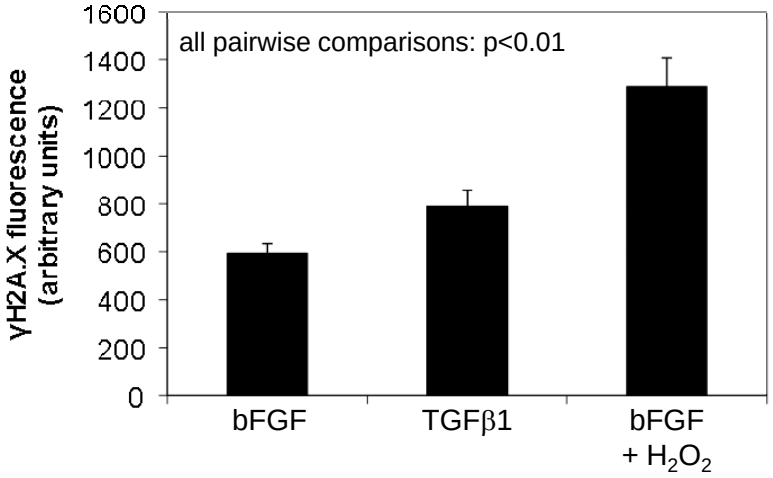
all pairwise comparisons: p<0.01
γH2A.X fluorescence (arbitrary units)
1600
1400
1200
1000
800
600
400
200
0
bFGF
TGFβ1
bFGF + H2O2

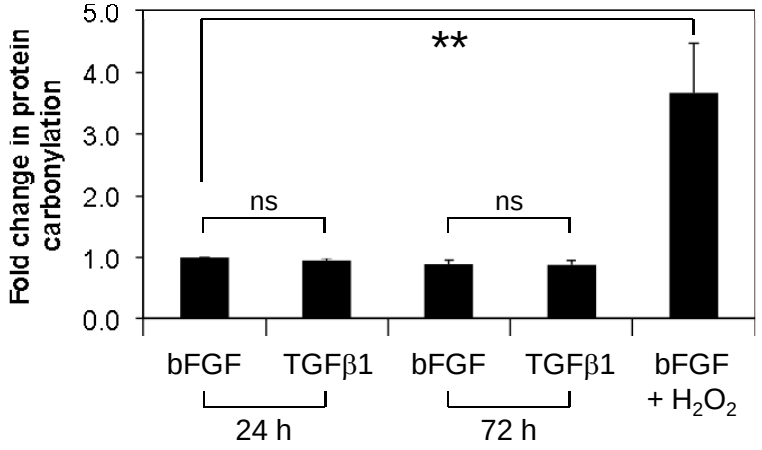
**
ns
ns
Fold change in protein carbonylation
5.0
4.0
3.0
2.0
1.0
0.0
bFGF
TGFβ1
bFGF
TGFβ1
bFGF + H2O2
24 h
72 h

Fig. 3

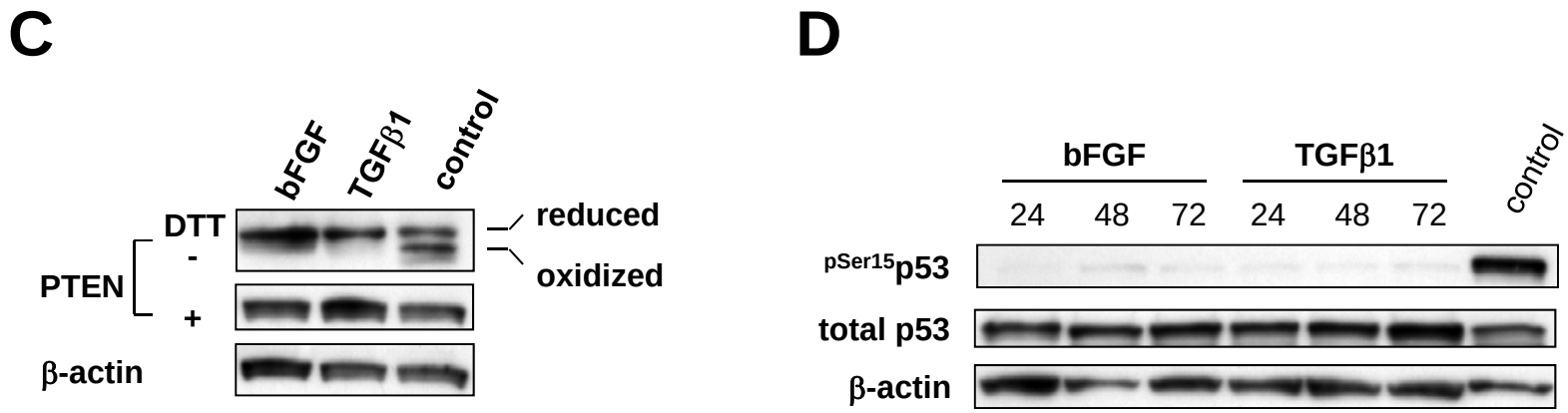
C
bFGF
TGFβ1
control
DTT
-
+
PTEN
β-actin
reduced
oxidized
D
bFGF
TGFβ1
control
24
48
72
24
48
72
pSer15p53
total p53
β-actin

Fig. 4

A

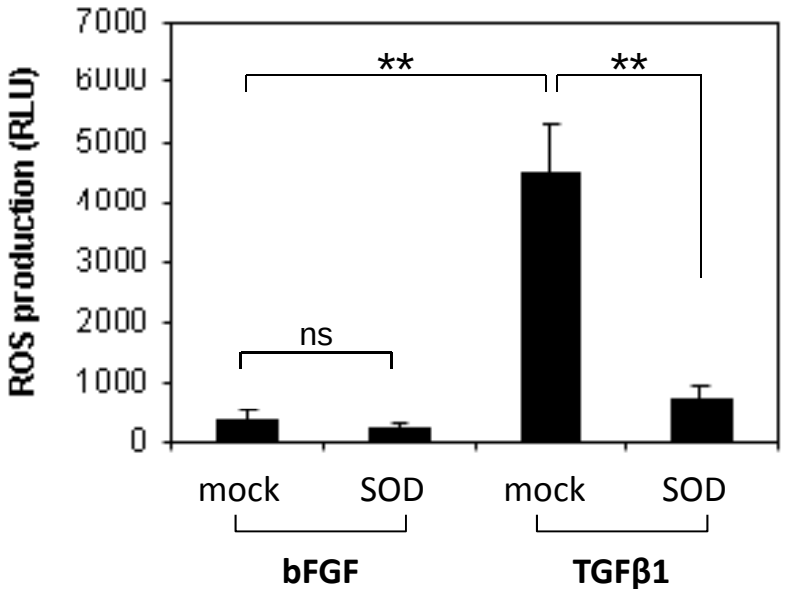
ROS production (RLU)
7000
6000
5000
4000
3000
2000
1000
0
**
**
ns
mock
SOD
mock
SOD
bFGF
TGFβ1

B

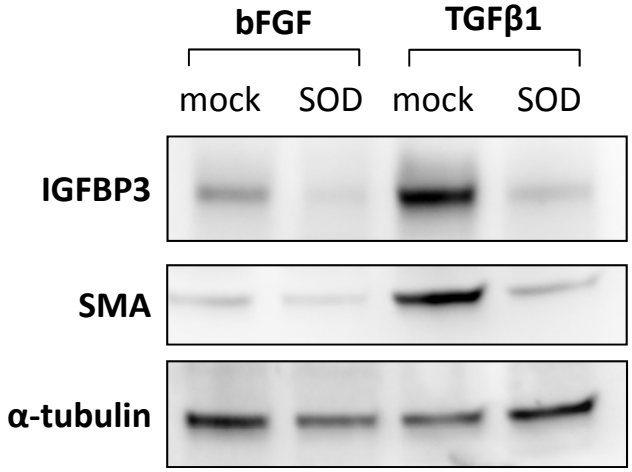
bFGF
TGFβ1
mock
SOD
mock
SOD
IGFBP3
SMA
α-tubulin

C

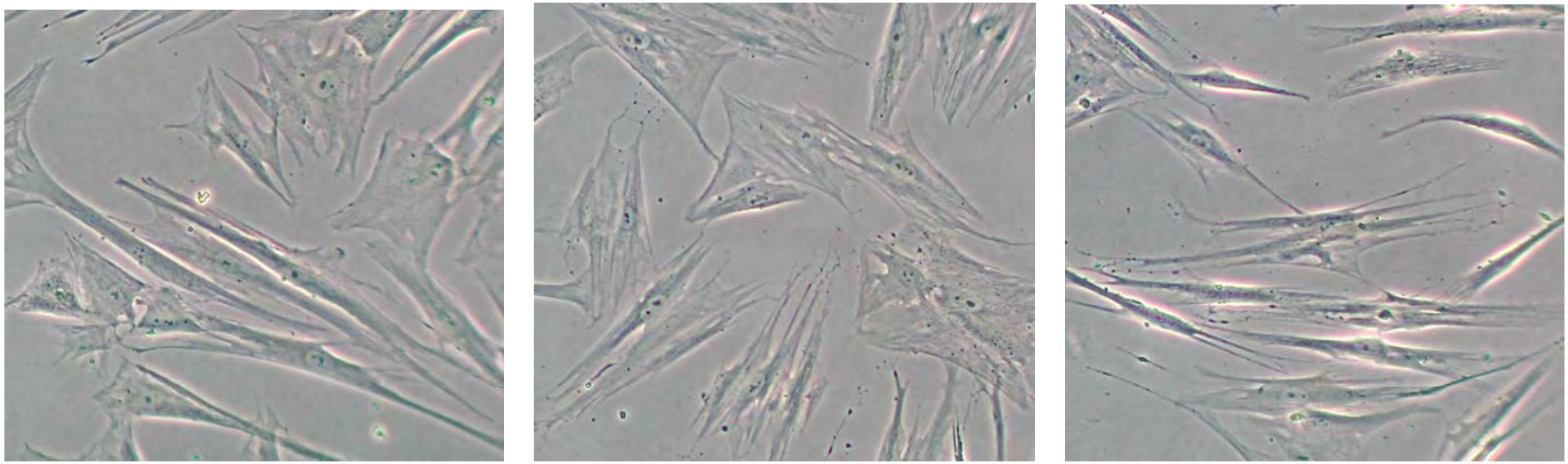
bFGF
TGFβ1
TGFβ1 + SOD

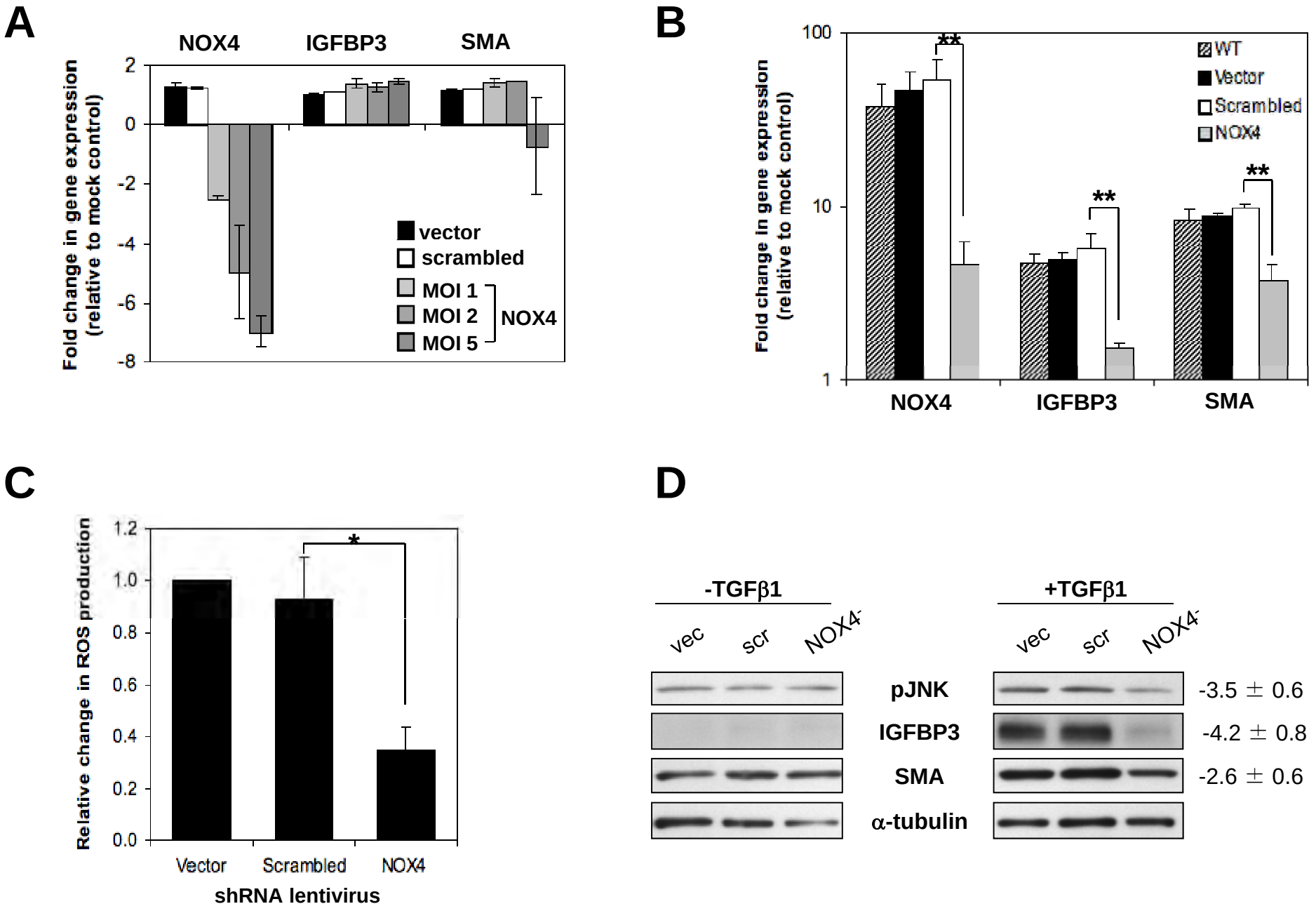
A
NOX4
IGFBP3
SMA
Fold change in gene expression (relative to mock control)
2
0
-2
-4
-6
-8
vector
scrambled
MOI 1
MOI 2
MOI 5
NOX4
B
100
10
1
**
**
**
WT
Vector
Scrambled
NOX4
Fold change in gene expression (relative to mock control)
NOX4
IGFBP3
SMA
C
Relative change in ROS production
1.2
1.0
0.8
0.6
0.4
0.2
0.0
*
Vector
Scrambled
NOX4
shRNA lentivirus
D
-TGFβ1
+TGFβ1
vec
scr
NOX4
vec
scr
NOX4
pJNK
IGFBP3
SMA
α-tubulin
-3.5 ± 0.6
-4.2 ± 0.8
-2.6 ± 0.6

Fig.5

Fig.5

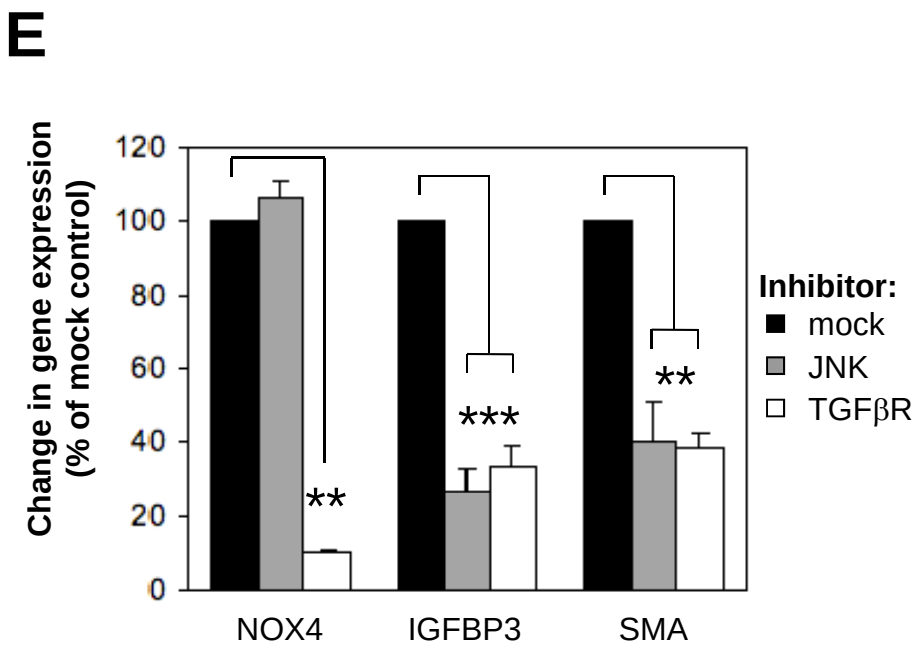
E
Change in gene expression
(% of mock control)
120
100
80
60
40
20
0
**
***
**
NOX4
IGFBP3
SMA
Inhibitor:
mock
JNK
TGFβR

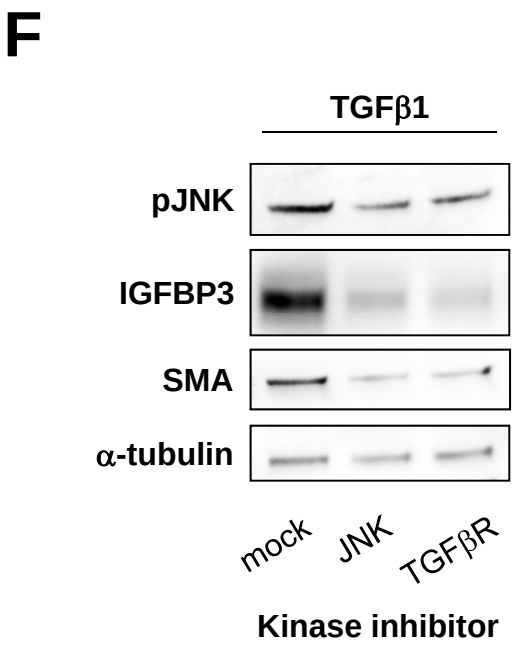
F
TGFβ1
pJNK
IGFBP3
SMA
α-tubulin
mock
JNK
TGFβR
Kinase inhibitor

A

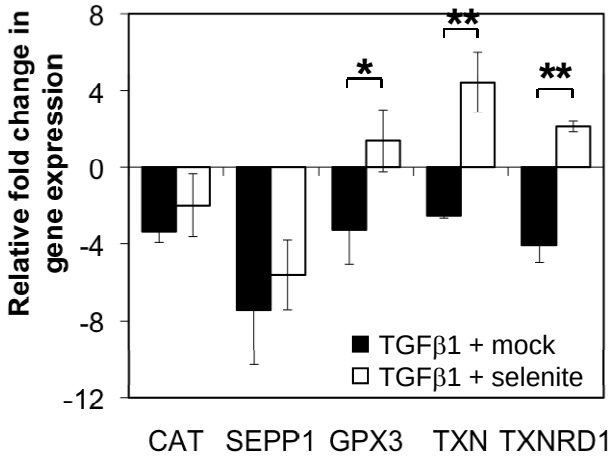
Relative fold change in gene expression
8
4
0
-4
-8
-12
*
**
**
TGFβ1 + mock
TGFβ1 + selenite
CAT
SEPP1
GPX3
TXN
TXNRD1

B

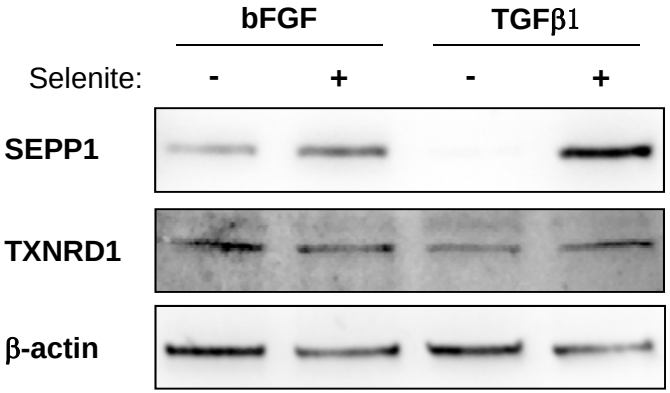
bFGF
TGFβ1
Selenite:
-
+
-
+
SEPP1
TXNRD1
β-actin

C

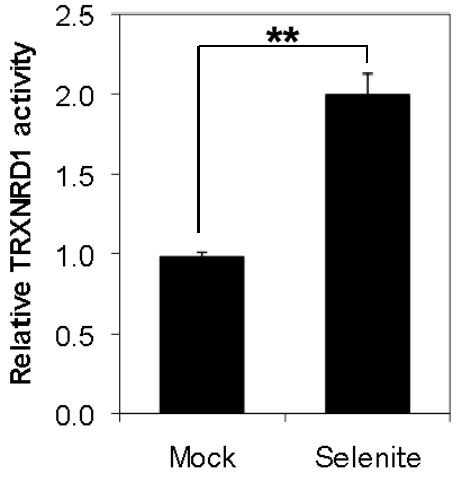
Relative TRXNRD1 activity
2.5
2.0
1.5
1.0
0.5
0.0
**
Mock
Selenite

Fig.6

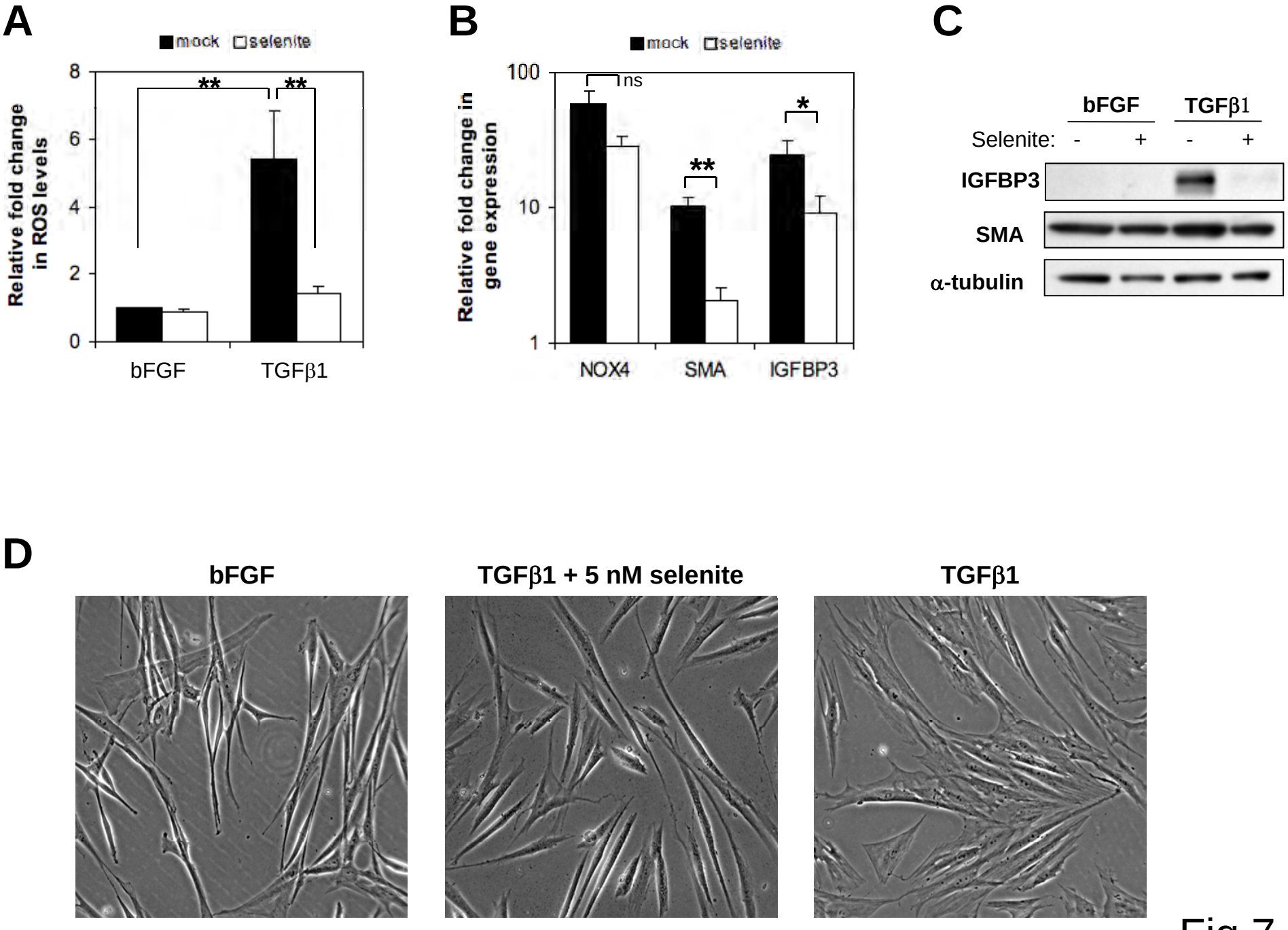
A
mock
selenite
Relative fold change in ROS levels
8
6
4
2
0
**
**
bFGF
TGFβ1
B
mock
selenite
Relative fold change in gene expression
100
10
1
ns
**
*
NOX4
SMA
IGFBP3
C
bFGF
TGFβ1
Selenite: - + - +
IGFBP3
SMA
α-tubulin
D
bFGF
TGFβ1 + 5 nM selenite
TGFβ1

Fig.7

Description	Gene symbol	Mean fold change[a]	SEM
Extracellular matrix component, tissue remodeling			
ADAM metallopeptidase with thrombospondin type 1 motif, 1	ADAMTS1	-22.50	8.39
ADAM metallopeptidase with thrombospondin type 1 motif, 19	ADAMTS19	-5.32	2.10
ADAM metallopeptidase with thrombospondin type 1 motif, 2	ADAMTS2	4.31	0.67
ADAM metallopeptidase with thrombospondin type 1 motif, 5	ADAMTS5	-4.29	1.15
ADAM metallopeptidase with thrombospondin type 1 motif, 6	ADAMTS6	9.15	1.00
biglycan	BGN	8.73	0.02
cadherin 2, type 1, N-cadherin	CDH2	7.29	0.75
cartilage oligomeric matrix protein	COMP	180.49	17.16
chondroitin sulfate proteoglycan 2 (versican)	CSPG2	6.46	2.03
collagen, type IV, alpha 1	COL4A1	21.06	1.29
collagen, type IV, alpha 2	COL4A2	9.51	0.48
collagen, type V, alpha 1	COL5A1	7.07	0.43
decorin	DCN	-5.24	1.41
desmoplakin	DSP	24.54	15.15
integrin, alpha 11	ITGA11	10.52	2.35
integrin, beta-like 1 (with EGF-like repeat domains)	ITGBL1	6.15	1.22
lysyl oxidase	LOX	3.94	0.52
lysyl oxidase-like 2	LOXL2	4.25	1.10
matrix Gla protein	MGP	11.17	3.35
membrane metallo-endopeptidase	MME	-7.10	0.54
microfibrillar-associated protein 2	MFAP2	17.19	3.92
neurofilament, light polypeptide 68kDa	NEFL	-15.00	1.86
pappalysin 2	PAPPA2	3.03	0.76
plasminogen activator, tissue	PLAT	-6.97	2.23
prostaglandin E synthase	PTGES	-21.49	1.02
sarcoglycan, gamma	SGCG	3.08	0.72
serpin peptidase inhibitor, clade B (ovalbumin), member 1	SERPINB1	-7.92	2.31
serpin peptidase inhibitor, clade E member 2	SERPINE2	19.65	8.79
serpin peptidase inhibitor, clade E member 1	SERPINE1	5.46	0.03
thrombospondin 1	THBS1	6.64	0.12
TIMP metallopeptidase inhibitor 3	TIMP3	7.16	1.77
Smooth muscle cell/myofibroblast markers			
actin, alpha 2, smooth muscle	ACTA2	13.32	4.23
caldesmon 1	CALD1	8.06	4.69
calponin 1, basic, smooth muscle	CNN1	12.99	1.71
phospholamban	PLN	344.95	89.14
tenascin	TNC	24.45	6.77
Growth factors			
connective tissue growth factor	CTGF	3.42	0.08
epidermal growth factor	EGF	14.08	4.54
fibroblast growth factor 1	FGF1	9.43	0.90
fibroblast growth factor 18	FGF18	7.86	0.52
heparin-binding EGF-like growth factor	HBEGF	68.54	3.27

pleiotrophin (heparin binding growth factor 8)	PTN	-3.29	0.67
Insulin-like growth factor axis			
insulin-like growth factor 1	IGF1	24.83	6.88
insulin-like growth factor 1 receptor	IGF1R	3.11	0.72
insulin-like growth factor binding protein 3	IGFBP3	9.53	2.75
insulin-like growth factor binding protein 5	IGFBP5	-6.78	0.69
insulin-like growth factor binding protein 7	IGFBP7	6.31	0.31
NUAK family, SNF1-like kinase, 1	NUAK1	9.43	1.04
Wilms tumor 1	WT1	-9.02	4.79
Transforming growth factor beta 1 axis			
cyclin-dependent kinase inhibitor 2B (p15)	CDKN2B	20.68	1.66
inhibin, beta E	INHBE	15.86	3.18
transforming growth factor, beta 1	TGFB1	5.31	2.07
transmembrane, prostate androgen induced RNA	TMEPAI	191.92	10.25
ROS production/scavenging			
catalase	CAT	-3.37	0.11
glutathione peroxidase 3	GPX3	-3.39	0.12
NAD(P)H dehydrogenase, quinone 1	NQO1	-5.57	0.59
NADPH oxidase 4	NOX4	436.57	20.75
neutrophil cytosolic factor 2 (p67phox)	NCF2	11.80	4.67
selenoprotein P 1	SEPP1	-7.18	0.16
superoxide dismutase 2, mitochondrial	SOD2	-7.11	0.00
thioredoxin reductase 1	TXNRD1	-3.99	0.20
Immune response			
collectin sub-family member 12	COLEC12	-56.56	21.61
complement component 3	C3	-15.70	9.15
interleukin 11	IL11	36.08	0.49
tumor necrosis factor superfamily, member 4	TNFSF4	7.38	0.22
Signal transduction/transcription factor			
cytokine receptor-like factor 1	CRLF1	35.24	3.51
early growth response 2	EGR2	72.83	16.67
EPH receptor A7	EPHA7	-17.85	10.76
neuronal PAS domain protein 3	NPAS3	-4.48	1.58
oxytocin receptor	OXTR	3.94	0.56
phosphodiesterase 1A, calmodulin-dependent	PDE1A	-6.49	1.76
Phosphodiesterase 5A, cGMP-specific	PDE5A	-8.59	1.60
plexin domain containing 2	PLXDC2	13.01	4.39
prostaglandin-endoperoxide synthase 1 (COX1)	PTGS1	5.36	1.35
RAB27B, member RAS oncogene family	RAB27B	-80.64	10.02
regulator of G-protein signalling 4	RGS4	5.55	0.04
runt-related transcription factor 1	RUNX1	7.92	2.30
secreted frizzled-related protein 1	SFRP1	-5.83	0.26
serologically defined colon cancer antigen 33	SDCCAG33	9.61	0.42
tetraspanin 13	TSPAN13	16.13	2.22
tetraspanin 2	TSPAN2	120.84	0.98
Transport			
aquaporin 1	AQP1	83.85	37.05
potassium inwardly-rectifying channel, subfamily J, member 2	KCNJ2	-28.42	10.56
solute carrier family 39 (zinc transporter), member 8	SLC39A8	-3.42	0.21
Miscellaneous/unknown			

	LOC541469	10.58	1.54
	FLJ37228	-12.85	0.48
alcohol dehydrogenase IB (class I), beta polypeptide	ADH1B	-13.26	5.91
ankyrin repeat domain 37	ANKRD37	7.19	2.34
carbonic anhydrase XII	CA12	-13.55	3.51
chromosome 10 open reading frame 116	C10orf116	-5.43	0.64
chromosome 5 open reading frame 13	C5orf13	4.31	2.23
hect domain and RLD 6	HERC6	-5.64	0.38
hydroxysteroid (11-beta) dehydrogenase 1	HSD11B1	-8.44	2.91
interferon-induced protein with tetratricopeptide repeats 3	IFIT3	-8.97	0.28
suppression of tumorigenicity 7 like	ST7L	-13.09	6.28
transmembrane protein with EGF-like and two follistatin-like domains 2	TMEFF2	-11.06	3.65
X-ray repair complementing defective repair in Chinese hamster cells 4	XRCC4	17.11	2.26

PrSCs from three independent donors were treated with 1 ng/ml TGFβ1 or 1 ng/ml bFGF for 48 h. Pooled RNA was hybridized to Affymetrix Human Genome U133 Plus 2.0 GeneChips®.
[a] Values represent mean fold change in expression relative to bFGF control cells from two independent hybridizations

Supplementary Table 1 Most highly regulated genes during TGFβ1-mediated transdifferentiation of primary human prostatic stromal cells.

Gene Symbol	Gene ID	Primer sequence[a]
ACTG2 (SMA)	72	F: AGAAGAGCTATGAGCTGCCA R: GCTGTGATCTCCTTCTGCAT
CAT	847	F: CGTGCTGAATGAGGAACAGA R: CAGATTTGCCTTCTCCCTTG
CDH1	999	F: ATTGCAAATTCCTGCCATTC R: GCTGGCTCAAGTCAAAGTCC
CNN1	1264	F: GGTGAACGTGGGAGTGAAGT R: GGTCCAGAGGCTGGTCTGT
COL4A1	1282	F: CCGGATTGAAAGGAGATCAA R: GCCTGGATCTTCTCACCTTG
COMP	1311	F: GGAGATCACGTTCCTGAAAA R: GGTGTTGATACAGCGGACTC
CORO2A	7464	F: GAGCCCATCTCCATGATTGT R: GGGCCATGGAATTGAAGATA
CYBA ($p22^{phox}$)	1535	F: GTCCTGCATCTCCTGCTCT R: ACAGCCGCCAGTAGGTAGA
DPP4	1803	F: CGTTACATGGGTCTCCCAAC R: CAGGGCTTTGGAGATCTGAG
DUSP1	1842	F: CTGCCTTGATCAACGTCTCA R: ACCCTTCCTCCAGCATTCTT
DUSP2	1844	F: GTGGAGATCAGTGCCTGGTT R: ACAGCACCTGGGTCTCAAAC
DUSP6	1848	F: CCTGGAAGGTGGCTTCAGTA R: GTTGGACAGCGGACTACCAT
DUSP10	11221	F: TGAATGTGCGAGTCCATAGC R: GTTGCAGAGCCAAGGTAAC
EHF	26298	F: AACCCGAGAGGGACTCACTT R: ACCAGTCTTCGTCCATCCAC
GPX3	2878	F: CCCTCAAGTATGTCCGACCA R: CAGAAGAGGCGGTCAGATGT
HMBS	3145	F: CCAGGACATCTTGGATCTGG R: ATGGTAGCCTGCATGGTCTC
IGF1	3479	F: GGAGGCTGGAGATGTATTGC R: GATGTGTCTTTGGCCAACCT
IGFBP3	3486	F: CAAGCGGGAGACAGAATATG R: TTATCCACACACCAGCAGAA
KLK2	3817	F: GTGGACACCTGTGTCAGCAT R: TGTGCCCATCCATGACTGTA
KLK3 (PSA)	354	F: TTGACCCCAAAGAAACTTCA R: TGACGTGATACCTTGAGGCA
KRT5	3852	F: AGGAGCTCATGAACACCAAG R: CCAGAGGAAACACTGCTTGT
NCF2 ($p67^{phox}$)	4688	F: GAGAACACAGTGGGTGACCA R: AGGTCCTCTGGTTGGGTAG
NOX1	27035	F:TGGTCATGCAGCATTAAACTTTG R: CATTGTCCCACATTGGTCTCC
NOX4	50507	F: TGGCAAGAGAACAGACCTGA R: TGGGTCCACAACAGAAAACA
NOX5	79400	F: CCCTTTGCTTCCATTCTG R: TCACAAACCACTCGAAAGA
OGN	4969	F: GCCTCTGATAAAGCCAGCAC R: ACGTGGGCATTTCATCATTT
PAGE4	9506	F: AATGGATCTGAAAAAGACTCG R: GTGACATCAGCCATGTGTGTA
PLN	5350	F: ACAGCTGCCAAGGCTACCTA R: GCTTTTGACGTGCTTGTTGA
PTP1B (PTPN1)	5770	F: GAATCCTGGAGCCACACAAT R: TTGACTCATGCTTTCGATGC
RARRES1	5918	F: TCATCTGGGATTTGGCTTTC

RARRES1	5918	F: TCATCTGGGATTTGGCTTTC R: CCAGGGTACCAGACCAAGTG
SEPP1	6414	F: TGGAAACTGCTCTCTCACGA R: GCTCCTGGTTGCTGATTCTC
SOD2	6648	F: TCCACTGCAAGGAACAACAG R: TCTTGCTGGGATCATTAGGG
TGFB1I1	7041	F: GCTTCAGGAACTTAATGCCA R: GAAGTCAGAGAGTGAGGCCA
TMPRSS2	7113	F: GGCTTTGAACTCAGGGTCAC R: GGTAGTACTGAGCCGGATGC
TNC	3371	F: GGAAACAAGAGCAGGACCAG R: CAGACAGCCAATGCTTCAGA
TXN	7295	F: CTGCTTTTCAGGAAGCCTTG R: ACCCACCTTTTGTCCCTTCT
[a] Primer sequences are given 5' to 3', annealing temperature for all		

Supplemental Table 2 Primer sequences